Assessing the Extent of Potential Inversion by Cyclic Voltammetry: Theory, Pitfalls, and Application to a Nickel Complex with Redox-Active Iminosemiquinone Ligands

Cheriehan Hessin, Jules Schleinitz, Nolwenn Le Breton, Sylvie Choua, Laurence Grimaud, Vincent Fourmond, Marine Desage-El Murr, Christophe Léger

Assessing the extent of potential inversion by cyclic voltammetry: theory, pitfalls, and application to a nickel complex with redox-active iminosemiquinone ligands

Cheriehan Hessin (a), Jules Schleinitz (b), Nolwenn Le Breton (a), Sylvie Choua (a), Laurence Grimaud (b), Vincent Fourmond (c), Marine Desage-El Murr *(a), Christophe Léger *(c)
(a) Université de Strasbourg, Institut de Chimie, UMR CNRS 7177, 67000 Strasbourg, France
(b) Laboratoire des Biomolécules, Département de Chimie, Sorbonne Université, École Normale Supérieure, PSL University, CNRS, 75005 Paris, France
(c) Laboratoire de Bioénergétique et Ingénierie des Protéines. CNRS, Aix Marseille Université, 13009 Marseille, France
* leger@imm.cnrs.fr, desageelmurr@unistra.fr

Abstract

Potential inversion refers to the situation where a protein cofactor or a synthetic molecule can be oxidized or reduced twice in a cooperative manner, that is the second electron transfer (ET) is easier than the first. This property is very important regarding the catalytic mechanism of enzymes that bifurcate electrons and the properties of bidirectional redox molecular catalysts that function in either direction of the reaction with no overpotential. Cyclic voltammetry is the most common technique for characterizing the thermodynamics and kinetics of ET to or from these molecules. However, a gap in the literature is the absence of analytical predictions to help interpret the values of the voltammetric peak potentials when potential inversion occurs ; the cyclic voltammograms are therefore often analyzed by simulating the data, with no discussion of the possibility of overfitting and often no estimation of the error on the determined parameters. Here we formulate the theory for the voltammetry of freely-diffusing or surface-confined two-electron redox species in the experimentally relevant irreversible limit where the peak separation depends on scan rate. We explain why the model is intrinsically underdetermined, and we illustrate this conclusion by the analysis of the voltammetry of a Ni complex with redox-active iminosemiquinone ligands. Being able to characterize the thermodynamics of two-electron transfer reactions will be crucial for designing more efficient catalysts.

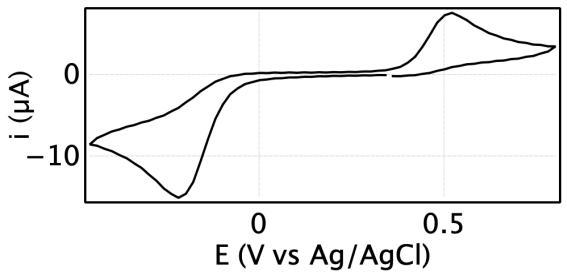

Redox molecules that undergo cooperative two-electron electron transfers are key to the development of the multielectron catalysts needed for efficient small molecule activation and electron storage. We revisit the voltammetric characterization of these systems, by proposing a theoretical framework and a data analysis method, which we apply to an experimental case. We explain why obtaining a set of parameters that gives a good fit of the voltammograms is not enough to reliably estimate potential inversion.

Correction: the X-axis of the TOC figure and figures 6A, 7A, S9A and S11A was incorrectly labeled "E (V vs SHE)" instead of "E (V vs Ag/AgCl)" in the initial version of this manuscript. It is corrected here.

Introduction

Many molecules can undergo multiple electron transfers. The particular case of two-electron redox processes is frequent in biology, because many biological redox reactions involve two electrons, and are catalyzed by enzymes that use two-electron redox sites ; the enzyme-catalyzed one-, four-, six- or eight-electron transformations of nitrite to nitric oxide, dioxygen to water, and nitrite or dinitrogen to ammonium, respectively, are important exceptions. The design of solar-fuels catalysts for the two-electron reduction of CO_2 or for the production or oxidation of H_2 has also attracted much attention in the last decade. In all cases, controlling the thermodynamics of electron or hole accumulation is needed to understand and optimize the properties of these catalysts.

As a result of electrostatics, any extra addition or removal of an electron to a molecule should be more difficult than the previous electron transfer. If we note with subscripts 1 and 2 the 1st and 2nd *reductions* that take a fully oxidized molecule (**O**) to the intermediate (**I**) and reduced (**R**) states,

$$\mathrm{O} + 1e^- \rightleftharpoons \mathrm{I} \quad E_1^0 \quad (1)$$

$$\mathrm{I} + 1e^- \rightleftharpoons \mathrm{R} \quad E_2^0 \quad (2)$$

$$\Delta E^0 = E_1^0 - E_2^0 \quad (3)$$

we expect that Coulombic repulsions should make the reduction potential of the 2nd reduction lower than that of the 1st (that is, $\Delta E^0 = E^0_1 - E^0_2 > 0$). However, various effects may destabilize the intermediate redox state, and ΔE^0 may be negative if one or both of the redox steps are coupled to structural changes or chemical reactions which compensate for the electrostatics.[1,2] Here we use the expression "potential inversion" to refer to the situation where ΔE^0 is either slightly positive or negative, so that the intermediate redox state is unstable. If ΔE^0 is sufficiently negative, the redox reaction is essentially a cooperative two-electron transfer.

According to the notation defined by eqs 1-3 and used throughout this paper, the more negative ΔE^0, the larger the extent of potential inversion, irrespective of the initial redox state of the system and the direction of the reaction (reduction during the downward sweep, oxidation in the upward sweep). However, this notation is arbitrary: in other papers in the literature, the subscripts in E^0_1 and E^0_2 refer to the 1st and 2nd *oxidations* of the two-electron reduced species, in which case the more positive ΔE^0, the greater the potential inversion.

A fundamental biological process where potential inversion is usually considered crucial is electron bifurcation, as occurs in mitochondrial cytochrome bc_1 and other enzymes where a quinone or a flavin cofactor transfers electrons to two different acceptors, the first one at high potential and the other at low potential. The thermodynamics and kinetics of the electron transfers are apparently finely tuned to prevent short-circuit,[3–6] although a recent, alternative view on electron bifurcation suggests that potential inversion may not be a requirement.[7] Regarding the design of bidirectional redox catalysts of two-electron redox reactions, engineering potential inversion is required in certain catalytic mechanisms to make the system energetically efficient. Indeed, if reductive and oxidative catalysis depend on the formation of the fully oxidized and reduced forms of the catalyst, respectively, decreasing $E^0_1 - E^0_2$ brings the oxidative and reductive catalytic waves closer to one another, to the point that catalysis may become fast in response to even a small difference between

the electrode potential and the equilibrium potential.[8–10] For example, the catalytic cycle of CO_2/formate conversion in acetonitrile by $[Pt(depe)_2]^{2+}$ (depe=1,2-bis(diethylphosphino)ethane) includes a cooperative two-electron transfer step.[11–13]

Investigations of the determinants of potential inversion involve the measurements of the two reduction potentials of the molecule of interest, and how these potentials are modified by various effects such as coupled proton-transfer, ligand binding/release, ion pairing, solvation etc.[1,2]

Among the techniques that allow ΔE^0 to be measured, some rely on the equilibration of mixtures of **O**, **I** and **R**. For example, the change in Nernst potential when the ratio [**O**]/[**R**] is varied by fractional electrolysis can be analyzed to estimate ΔE^0 (ref [14]). In equilibrium redox titrations, which are very common in the characterization of protein cofactors, the concentration of **I** is measured using a spectroscopic technique as a function of the equilibrium potential, to determine E^0_1 and E^0_2 (fig 1A).[15] Alternatively, in characterizations of small, synthetic molecules, a straightforward method consists in equilibrating a mixture of **O** and **R** (each in concentration C_0), and measuring the resulting equilibrium concentration of **I**, which is related to ΔE^0 by eq. 4 :

$$[\mathrm{I}]/C_0 = \left(1 + 2\exp^{-F\Delta E^0/2RT}\right)^{-1} \quad (4)$$

This approach relies on the possibility to use a spectroscopic method to detect small amounts of the intermediate redox state,[16,17] but the latter is all the more small as ΔE^0 is negative (cf eq. 4 and fig 1B).

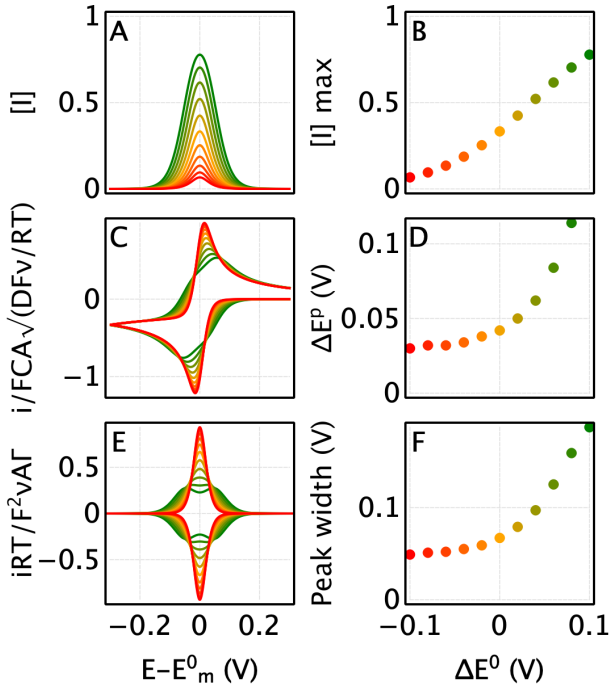

Figure 1. Measurement of potential inversion from the results of experiments where the redox species equilibrate: potentiometric titrations (A,B) and voltammetry under Nernstian conditions, with a diffusing (C,D) or adsorbed (E,F) species. We note $E^0_m = (E^0_1 + E^0_2)/2$. The data have been calculated with ΔE^0 ranging from 0.1 to -0.1 V (from green to red). Panel A: concentration of **I** as a function of the equilibrium electrode potential *E*. Panel B: maximal concentration of **I** against ΔE^0 (eq 4, see also table 11.1 in ref [2]). Panel C: reversible cyclic voltammograms of a freely-diffusing two-electron species (in the limit of infinitely slow scan rate), *i* is the current, *A* the electrode surface, C the total concentration of redox species in solution, *D* its diffusion coefficient, v the scan rate. Panel D: the corresponding peak separation as a function of ΔE^0 (see also ref [18] or the SI of ref [19]). Panel E: reversible cyclic voltammograms of an adsorbed two-electron species (in the limit of infinitely slow scan rate), Γ is the surface coverage.[20] Panel F: the corresponding peak

width at half height as a function of ΔE^0 (see also fig 10 in ref [21]).

Dynamic electrochemistry was often used to measure the two reduction potentials of small molecules. In voltammetric experiments, either the redox species is adsorbed onto an electrode or it freely diffuses in the solution that bathes the electrode, and the electrode potential (E) is swept up and down at a certain scan rate (v, in units of V/s). The redox processes are detected as current peaks (we count the reductive current as negative). Two-electron systems often give just one anodic and one cathodic peaks, revealing the two-electron oxidation and reduction of the molecule, respectively.

If it can be assumed that the system equilibrates with the electrode (e.g. if the scan rate is slow and the electron transfer rate fast), the peak potentials are independent of scan rate and the voltammogram is termed 'reversible' or 'Nernstian'. Two pairs of peaks are observed if ΔE^0 is large and positive, and a single pair of peaks is observed if ΔE^0 is small or negative (SI fig 1). If ΔE^0 is not too negative, the extent of potential inversion can be estimated by using working curves which relate ΔE^0 to either peak separation ΔE^p (if the species diffuse in solution, fig 1D) or to peak width (if the species is adsorbed onto the electrode, fig 1F). The peak widths of a signal obtained by differential pulse voltammetry of a species diffusing in solution, also under Nernstian conditions, give the same information.[22]

However, in most cases published in the literature, and in particular when the potential inversion was found to be large, the voltammetric signal was 'irreversible', showing two separated peaks whose positions depended on scan rate. This occurs when the rate of electron transfer is slow or the scan rate fast, so that the redox species are not in equilibrium with the electrode potential. The value of ΔE^0 was sometimes directly estimated from the peak separation,[23] or the value of the inverted potential directly from the peak position (as e.g. in the interpretation of the square wave voltammogram in ref [24]), and indeed it has been claimed that the two peak potentials should be "close to" the values of E^0 (see e.g. ref [2], p 406). We shall explain below that this is a misconception. In other papers, the values of ΔE^0 and the electron transfer rate constants were obtained from the analysis of the "trumpet plots" of peak positions against scan rate[19,25,26]. Most often, the same parameters were determined by simulating either one cyclic voltammogram (CV) or a set of CVs recorded at different scan rates with the simple two-electron model that we shall use herein.[2] Fitting this minimal model to the data requires adjusting a number of parameters: 2 E^0s, 2 rates of electron transfer (k_0), 2 transfer coefficients (α), at least one diffusion coefficient and the product of electrode surface times concentration. The unicity of the set of "best" parameters that comes out of the fitting procedures was rarely discussed. Very early on, Bard et al. questioned the "exact quantitative significance" of the parameters obtained from this type of simulations.[27] Kraiya et al. showed that ΔE^0 is well determined by the fitting procedure on condition that all other parameters are fixed,[28] but, in contrast, Hu et al.[29,30] (in particular table 1 in ref [30]) and Bellec et al.[19] reported some correlation between distinct values of ΔE^0 and of the electron transfer rate that provided a good fit of their voltammetric data, suggesting that these values are actually ill-defined. A systematic discussion of the accuracy of the data analysis was not possible, due to the absence of analytical predictions of the peak positions and peak shapes.

Here we describe the theory of two electron transfers in cyclic voltammetry for freely-diffusing or adsorbed two-electron species. We focus on the irreversible limit where the peak separation is large

and dependent on scan rate, which is experimentally relevant when potential inversion occurs ; we give the expressions of the peak positions and peak separations as a function of the parameters of the model, and we use these conclusions to explain why the fits are underdetermined to some extent. Our findings are supported by an analysis of the voltammetry of a Ni complex, which we synthesized and characterized using both voltammetry and spectroscopy. We propose a new method for analyzing the voltammograms that gives the *range* of ΔE^0 values that is consistent with a particular data set.

Peak positions in the cyclic voltammograms of two-electron redox species

Regarding the voltammetry of a two electron species, if the half reduced state **I** is stable over a large range of potential, the voltammetry consists of two independent one-electron pairs of peaks (SI fig S1), as described in many textbooks.[31,32]

Hereafter, we shall only describe the voltammetry when the potentials are "inverted" ($E^0_1 < E^0_2$) and **I** is unstable, which has not been clearly addressed in the literature: in particular, the equations that give the separation of the voltammetric peaks as a function of the parameter (E^0, scan rate etc.) for systems that undergo cooperative two-electron transfers ($E^0_1 < E^0_2$) have not been given. We focus on the most common situation where the redox molecule diffuses in solution to/from the electrode ; the equivalent equations for a molecule that is *adsorbed* onto an electrode are given in SI section S12.

We shall use the simplest and most common mechanism for a two-electron redox process, with the assumptions that have been used in most of the electrochemical literature on potential inversion.

Namely, we assume that the redox process is essentially a series of two one-electron transfers, and that the kinetics of the ET follows Butler-Volmer kinetics:[32,33]

$$\mathrm{O} \underset{k_1^{\mathrm{ox}}}{\overset{k_1^{\mathrm{red}}}{\rightleftarrows}} \mathrm{I} \underset{k_2^{\mathrm{ox}}}{\overset{k_2^{\mathrm{red}}}{\rightleftarrows}} \mathrm{R} \quad (5)$$

$$k_i^{\mathrm{red}} = k_{0i} \exp\left(-\frac{\alpha_i F}{RT}(E - E_i^0)\right) \quad (6)$$

$$k_i^{\mathrm{ox}} = k_{0i} \exp\left(\frac{(1-\alpha_i) F}{RT}(E - E_i^0)\right) \quad (7)$$

We note E the electrode potential.

If $\alpha_1 \approx \alpha_2$ and $k_{01} \approx k_{02}$, the relative thermodynamics of the two steps defines their relative rates: the more favorable the electron transfer, the greater its rate constant. There are cases where this approximation fails: ref [34] reports an experimental case where the two values of k_0 are very different, leading to unusually complex two-electron voltammetry with multiple peaks on each sweep, unlike the kind of data that we consider herein.

We assume that **O** and **R** are stable: the redox processes are not followed by any *irreversible* reaction. They may be coupled to *reversible* reactions, such as protonation and conformational changes ; we assume that these reactions are fast on the time scale of the voltammetry, hence they

do not need to be explicitly taken into account. Indeed, Laviron and coworkers have showed that redox reactions that are coupled to fast, reversible non-redox reactions such as proton transfers behave like pure electron transfer reactions, but in eqs. 6 and 7, the potentials E^0 and prefactors k_0 take apparent values that are affected by the thermodynamics of the fast coupled reactions.[35] The work in refs [36,37], for example, shows that explicitly taking into account the kinetics of the coupled reactions is not necessary if the simpler two-electron model gives a good fit of the data. Finally, in this theoretical section, we shall *neglect* the homogeneous disproportionation/comproportionation reaction.[38,39]

Each of the above hypotheses could be questioned on a case-by-case basis (and indeed, in the experimental part, we shall test whether or not the disproportionation reaction makes a difference to our conclusions), but the fact that *simple* assumptions allow one to reproduce voltammetric data acquired over a range of scan rates is usually a sufficient validation of the hypotheses.

Under these assumptions, in the "reversible" (or "Nernstian") limit, which is reached at infinitely slow scan rate, a single pair of peaks appears at $E^0_m = (E^0_1+E^0_2)/2$ if $E^0_1<E^0_2$ (red in fig 2A). The peak separation is independent of scan rate and equals 30 mV, and the average of the anodic and cathodic peak positions equals the value of the two-electron reduction potential $E^0_m = (E^0_1+E^0_2)/2$.[32,40]

As the scan rate is increased above a certain limit the separation between the anodic and cathodic peaks increases. We shall note ΔE^p this peak separation, $\Delta E^p = E^{pa} - E^{pc}$ (superscript "p" for "peak", "a" or "c" for "anodic" or "cathodic"). The faster the scan rate, the larger ΔE^p. In the "irreversible limit", the peak separation is large, so that the anodic and cathodic peaks do not overlap.

Figure 2A shows a series of cyclic voltammograms, started by a reductive sweep, calculated using digital simulations for increasing values of the ratio v/k_0^2 (from red, the reversible limit, to blue). Note the increase in peak separation at faster scan rates, and the dissymmetry of the signal: the initial reductive peak is larger than the reoxidation peak. This is because when the peak separation is greater, a larger fraction of the reduced species formed on the reductive sweep diffuses away from the electrode and cannot be reoxidized. This is clearly observed in experiments (e.g. see below).

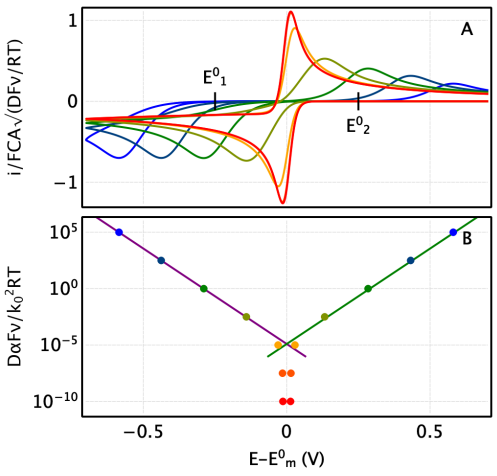

Figure 2 : Voltammetric signatures of a diffusing redox molecule that undergoes cooperative two-electron transfer. Panel A shows voltammograms calculated assuming $E^0_1-E^0_2$ = -0.5 V, $k_{02} = k_{01}$, $\alpha_1 = \alpha_2 = 0.5$, and v/k_0^2 increasing from red (reversible limit) to blue. We note $E^0_m = (E^0_1+E^0_2)/2$. Panel B shows the corresponding "trumpet plot" ; the circles indicate the peak positions obtained from the numerical simulations shown in panel A, and the lines predict the peak positions according to eqs 8 (purple) and 9 (green). SI fig S2 is identical except that it was calculated with $\alpha_1 = \alpha_2 = 0.6$, to show an example of a dissymmetrical trumpet plot.

The rest of this section focuses on the irreversible limit where the peak separation is large and depends on scan rate.

We show below that the positions of the 2 peaks observed for irreversible two-electron reactions with $E^0_1 < E^0_2$ are simply obtained from the equations derived by Nicholson and Shain for one-electron redox transformations[40]. Figure 2 compares the predicted peak positions and those obtained from numerical simulations of the redox system (lines and dots in fig 2B, respectively).

During the reductive sweep, the irreversible reduction of **O** to **I** occurs at at

$$E^{\mathrm{pc}} = E^0_1 - \frac{RT}{\alpha_1 F}\left(0.780 + \ln\sqrt{D_{\mathrm{O}}\alpha_1 F\nu/k^2_{01}RT}\right) \quad (8)$$

(cf the purple line in fig 2B). It is followed by the reduction of **I** to **R**, and we expect this second step to be fast because of the very favorable thermodynamics : $E_1^{pc} << E^0_2$, therefore $k_2^{red} >> k_1^{red}$ at low potential. This fast, irreversible, follow-up reduction doubles the magnitude of the cathodic peak, but it changes neither its position nor its shape, because the **O**-to-**I** step is rate-determining. Therefore the second reduction (**I** to **R**) does not appear as a second peak on the reductive sweep.

On the return sweep, a unique anodic, irreversible peak is seen when **R** is reoxidized to **I**, at

$$E^{\mathrm{pa}} = E^0_2 + \frac{RT}{(1-\alpha_2)F}\left(0.780 + \ln\sqrt{D_{\mathrm{O}}(1-\alpha_2)F\nu/k^2_{01}RT}\right) \quad (9)$$

This ET is followed by the very favorable and very fast oxidation of **I** to **O**, so that a single oxidative peak is observed.

Note that the average of the peak potentials equates the two-electron reduction potential $E^0_m = (E^0_1+E^0_2)/2$ only if $D_O = D_R$, $\alpha_1 = 1-\alpha_2$ and $k_{01} = k_{02}$.

The values of E^{pc} (eq 8) and E^{pa} (eq 9) are plotted as purple and green lines in the "trumpet plots" in fig 2B, and match the positions of the peaks measured in simulations (dots in fig 2B).

The peaks shift upon increasing the scan rate:

$$\mathrm{d}\ E^{\mathrm{pc}}/\mathrm{d}\ \log_{10}(\nu) = -2.3RT/2\alpha_1 F \quad (10)$$

$$\mathrm{d}\ E^{\mathrm{pa}}/\mathrm{d}\ \log_{10}(\nu) = 2.3RT/2(1-\alpha_2)F \quad (11)$$

The two slopes of the trumpet plot are around 60 mV/decade if α_1 and $\alpha_2 \approx 0.5$.

The scan rate above which the irreversible anodic and cathodic peaks separate is calculated from eqs 8 and 9. Assuming for the sake of simplicity that $D_O = D_R$, $k_{02} = k_{01}$ and $\alpha_1 = \alpha_2 = 0.5$, we obtain

$$\nu_{\mathrm{split}} = \frac{k_0^2 RT}{D\alpha F}\exp\left(\frac{\alpha F}{RT}(E^0_1 - E^0_2) - 2\times 0.78\right) \quad (12)$$

The system is in the irreversible limit (and eqs 8-14 are valid) only when $v > v_{split}$.

Equation 12 has a major implication regarding the positions of the peaks with respect to the thermodynamic potentials E^0 and the meaning of the peak separation. For a one-electron system, the position of the reductive peak position is

$$E^{\mathrm{pc}} = E^0 - \frac{RT}{\alpha F}\left(0.780 + \ln\sqrt{D\alpha F\nu/k_0^2 RT}\right) \quad (13)$$

and peak separation is observed if $v > k_0^2 RT/D\alpha F$; this implies that the reductive peak is at *lower* potential than E^0. In contrast, for a two-electron system with inverted potentials, peak splitting may be observed even if $v < k_0^2 RT/D\alpha F$, because the exponential term in eq 12 is much smaller than one.

Therefore, the logarithmic terms in eqs 8 and 9 may be positive or negative. As a consequence, the cathodic peak occurs at a potential that may be either greater or lower than E^0_1, depending on scan rate: see e.g. in fig 2B how the position of the cathodic peak (purple line) compares with the value of E^0_1.

The peak separation $\Delta E^p = E^{pa} - E^{pc}$ (obtained from eqs 8 and 9 *in the irreversible limit* assuming $\alpha_1 = \alpha_2 = 0.5$ and and $k_{01} = k_{02}$) has a large thermodynamic contribution $E^0_2 - E^0_1$, in addition to the scan-rate dependent kinetic contribution :

$$\Delta E^p = \underbrace{E_2^0 - E_1^0}_{\text{thermodynamics}} + \underbrace{\frac{RT}{\alpha F}\left(2 \times 0.78 + \ln \frac{D\alpha F\nu}{k_0^2 RT}\right)}_{\text{kinetics}} \quad (14)$$

The sign of the kinetic contribution may be positive or negative, and therefore the peak separation can be greater or lower than ΔE^0, it is not a proxy of the potential inversion:

$$\Delta E^p \neq -\Delta E^0 \quad (15)$$

This combination of thermodynamic and kinetic contributions (1st and 2nd terms in the right hand side of eq 14, respectively) causes the indetermination of the fits that is described in the next section.

Implications regarding the fitting of the voltammograms when potential inversion occurs

The previous section shows that by examining peak positions alone, or how peak positions depend on scan rate, the extent of potential inversion and the values of k_0 cannot be unambiguously measured. This is because a large inversion (negative ΔE^0) or slow interfacial electron transfer kinetics (small k_0) have the same effect on peak separation and cannot be distinguished (eq 14). The method for measuring ΔE^0 by voltammetry often consists in fitting the two-electron model to a voltammogram, instead of just looking at peak positions, or to a series of voltammograms recorded at different scan rates. Below we use this method on an experimental example to demonstrate that the indetermination remains even if the complete waveshape is considered, and we propose a systematic method that gives the *range* of values of ΔE^0 that is consistent with a particular data set.

The strategy that we shall use several times in the sections below consists in running series of constrained fits, and comparing the quality of the fits by looking at the value of the residuals (the residuals are the differences between the best fits and the data, the better the fits the smaller the residuals ; ref [41] is an introduction to fitting, which may be useful to readers who are not familiar with the concept). Our fits are 'constrained' because we adjust certain parameters of the model, while others (e.g. ΔE^0, the values of α, the disproportionation rate constant) are forced to take certain values ; this contrasts with the more common method that consists in running a single fit that returns the best value of all parameters. Comparing the quality of all the constrained fits allows us to define *ranges of parameter values* (not just parameter values) that are consistent with the data. In the 2D maps below (figs 8 and 9) we use a color code from green to red to indicate that the best fits are good or bad. If forcing a parameter to take any value within a large window of possible values makes no difference to the final quality of the fit, we conclude that this window gives the limits of the values of the parameter that are acceptable.

Synthesis and characterization of a model complex $[Ni(BQ)_2(Cl)_2]$ ($1^{2+}\cdot 2Cl^-$) with inverted potentials

Aminophenols are mono-aza-analogues of catechols and well-established redox-active structures.[42] Complexed to 3d metals such as Cu and Ni, these ligands form stable complexes in their iminosemiquinone (SQ) and benzoquinone (BQ) redox states. The resulting complexes perform electron transfer by favoring ligand-based redox changes from SQ to BQ, thus circumventing metal-based redox activity.[43] In this series, it has been shown that $Ni(SQ)_2$ **1**, a Ni^{II} complex derived from 2-anilino-4,6-di-*tert*-butylphenol, exhibits a 2-electron voltammetric wave when it is oxidized from $Ni(SQ)_2$ (**1**) to $Ni(BQ)_2^{2+}$ ($\mathbf{1}^{2+}$) in $TBAPF_6$ (TBA: tetrabutyl ammonium $[(n\text{-}Bu)_4N]^+$), which suggests that the two reduction potentials of this complex are inverted, making it a good model system in this work.

We investigated by UV-vis spectroscopy the oxidation of **1** with increasing amounts of ferrocenium chloride (**Fc·Cl**), a 1-electron oxidant. The UV-vis spectra show the conversion of **1** (879 nm) into the doubly oxidized species $[Ni(BQ)_2(Cl)_2]$ ($\mathbf{1}^{2+}\cdot 2Cl^-$) (448 nm) (fig 3). Complex $\mathbf{1}^{2+}\cdot 2Cl^-$ can be prepared from **1** in 37% overall yield by oxidation with silver triflate (AgOTf) followed by anion metathesis with *n*-tetrabutylammonium chloride ($n Bu_4NCl$) (fig 3). The structure of $\mathbf{1}^{2+}\cdot 2Cl^-$ was confirmed by crystallographic analysis as an octahedral complex with two chlorides ligated at the axial positions (SI section S5); representative bond lengths, angles and crystallographic parameters are included in SI Table S1. The UV-vis spectra of complex **1** and $\mathbf{1}^{2+}\cdot 2Cl^-$ shown in fig S3 are in agreement with the consumption of **1** for the benefit of $\mathbf{1}^{2+}\cdot 2Cl^-$ in fig 4.

The isosbestic point at 573 nm in fig 4 indicates that the reaction does not involve the formation of a stable singly reduced intermediate and that a 2e- transfer is favored. The examination by EPR of an equimolar mixture of **1** and $\mathbf{1}^{2+}\cdot 2Cl^-$ (1 mM) confirmed this observation, as no signal was detected at room temperature, which implies that the singly reduced $\mathbf{1}^+$ form is formed only in very small amounts, below the 1 µM detection limit (SI section S4). By using eq 4, we conclude that $\Delta E^0 < -140$ mV.

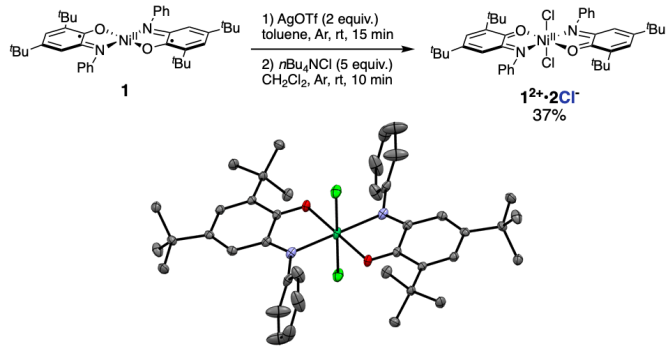

Figure 3. Synthesis and X-ray crystallographic structure of $[Ni(BQ)_2(Cl)_2]$ ($\mathbf{1}^{2+}\cdot 2Cl^-$), the doubly oxidized species from $Ni(SQ)_2$ **1**.

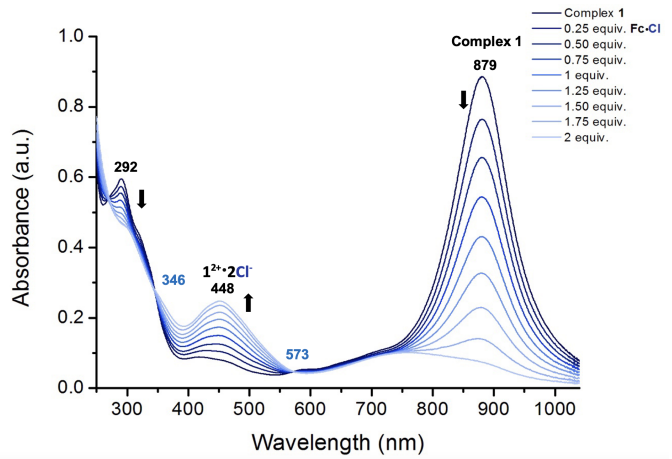

Figure 4. UV-vis absorption spectrophotometric titration of complex **1** (26 µM) with increasing amounts of **Fc·Cl** (0 to 2 equiv.) in degassed CH_2Cl_2.

Voltammetry of $[Ni(BQ)_2(Cl)_2]$ ($1^{2+}\cdot 2Cl^-$)

Figure 5 shows a series of cyclic voltammograms for the reduction and reoxidation of $[Ni(BQ)_2(Cl)_2]$ (**$1^{2+}\cdot 2Cl^-$**). All experiments described herein were performed on a stationary glassy-carbon electrode and using ohmic drop compensation. Panel B shows that the magnitude of the voltammetric peaks increases in proportion to $v^{1/2}$, this is because the complex freely diffuses in the solution that bathes the electrode.

The data in fig 5 were acquired using $TBABF_4$ as supporting electrolyte, but the data in supplementary Section S9 show that the quantitative conclusions from our analysis are the same when $TBABF_4$ is replaced with TBACl. Experiments in SI section S10, showing the voltammetry of the reduced $[Ni(SQ)_2]$ complex **1** in TBACl starting from the low potential limit, also gave similar results. These experiments suggest that the oxidative and reductive peaks correspond to the same two-electron transformation. Moreover, the analysis below shows that the above-described two-electron model, which is most commonly used in the context of potential inversion, describes well the shape of the voltammograms and their dependence on scan rate, suggesting that the reaction kinetics is indeed simple and that using a more complex model is not justified.

Figure 5C shows that the oxidative and reductive peaks shift in proportion to ln(v). According to the above results, the cathodic peak corresponds to the 1st reduction of the complex, at a potential given by eq 8, and the slope of the cathodic part of the trumpet plot gives $\alpha_1 = 0.5$ (eq 10). Similarly, from the anodic branch and eq 11 we calculate $\alpha_2 = 0.3$.

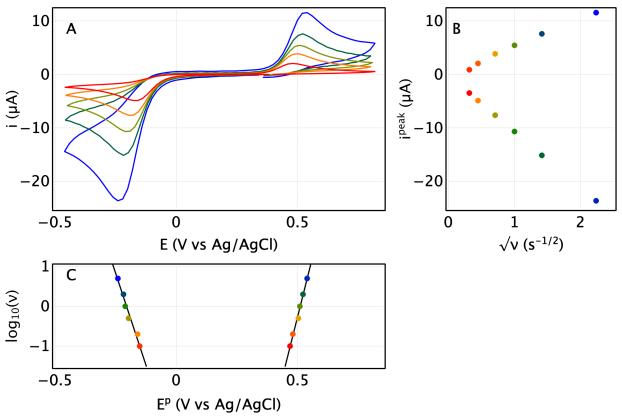

Figure 5. Voltammetry of $[Ni(BQ)_2(Cl)_2]$ ($\mathbf{1^{2+}\cdot 2Cl^-}$). Panel A: CVs recorded in the range 0.1 to 5 V/s (from red to blue), with $\mathbf{1^{2+}\cdot 2Cl^-}$ (C = 1 mM) in CH_2Cl_2 + 0.1 M $TBABF_4$, on a glassy carbon electrode (A = 0.8 mm^2), at T = 25°C. The potentials are quoted versus Ag/AgCl (KCl 3 M). Panel B: the linear change in peak current against square root of scan rate. Panel C: trumpet plot of peak positions against scan rate on a log scale. The fit of a straight line to each branch (based on eqs 10 and 11) gave $\alpha_1 = 0.5$ and $\alpha_2 = 0.3$.

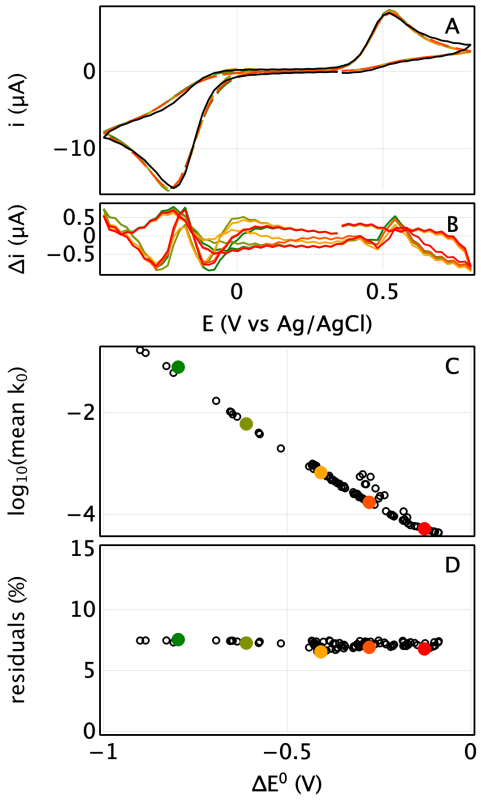

Figure 6. Underdetermination of the fitting of the voltammetry of $[Ni(BQ)_2(Cl)_2]$ ($\mathbf{1^{2+}\cdot 2Cl^-}$) shown in Figure 5A.
Panel A: the 2 V/s CV of $[Ni(BQ)_2(Cl)_2]$ ($\mathbf{1^{2+}\cdot 2Cl^-}$) (black, same conditions as in fig 5), overlaid with 5 different fits out of 500 results (green to red, they are almost indistinguishable).
Panel B: residuals of the fits shown in Panel A.
Panel C: plot of the geometric mean electron transfer rate constant ($\sqrt{(k_{01}k_{02})}$) against the final (best) value of ΔE^0, for the 100 best fits of the CV with initial parameters randomly chosen in the range: $(E^0_1+E^0_2)/2 \in$ [0-0.4V], $\Delta E^0 \in$ [-0.6-0.1V], k_{01} and $k_{02} \in [10^{-8}$-1 cm/s] (on a log scale), $AC \in$ [6-9 10^{-6} mol/cm], $\alpha_1 = 0.5$, $\alpha_2 = 0.3$, $D = 9\ 10^{-6}$ cm^2/s (see text). The five colored points correspond to the five fits shown in panel A.
Panel D: relative residuals of the 100 best fits described above.

The model depends on 8 parameters — E^0_1, E^0_2, k_{01}, k_{02}, α_1, α_2, D (the diffusion coefficient, which was assumed to be the same for all three redox states), and AC (A is the electrode surface, C the concentration, the product $AC(D)^{1/2}$ defines the overall magnitude of the signal) — plus temperature and scan rate. We used the in-house program QSoas[44] to search for the best values of the parameters of the model by fitting the result of digital simulations (see methods) to the experimental data. To fully explore the parameter space we used a feature of QSoas that randomly selects a large number (typically, hundreds) of initial "seeds" (a set of initial parameters, each parameter either fixed to a certain value or randomly chosen within a certain range) and uses an optimization algorithm to

adjust the parameters until a best agreement between the data and the simulation is found. The outcome of the procedure is a large number of sets of best parameters, each corresponding to a certain constraint, a certain seed and a certain final simulation, the quality of which is assessed by examining the value of the total residual (the distance between the fit and the data).

In a first exploration, we ran 500 fits of one of the CVs in fig 5A (the one recorded at 2 V/s), each starting from a seed defined by $(E^0_1+E^0_2)/2 \in 0$ to -0.4V, ΔE^0 = -0.6 to -0.1V, k_{01} and $k_{02} = 10^{-8}$ to 1 cm/s (on a log scale), AC = 6 to 9 10^{-6} mol/cm, and adjusting these 5 parameters until "best values" were obtained, keeping the other three parameters fixed: $\alpha_1 = 0.5$, $\alpha_2 = 0.3$ (deduced from fig 5C), $D = 9\ 10^{-6}$ cm^2/s (determined by DOSY, see methods section S6). Figure 6A shows 5 selected fits out of the 500, and Panel B shows the 5 corresponding residuals (the differences between the data and each simulation). The 5 fits are equally good (either judging by the eye, or from the values of the total residuals in panel D, which are all within 15 % of each other). However, the 5 best values of ΔE^0 range from -125 to -800 mV, showing that this parameter cannot be identified by the fitting procedure. The best values of k_0 also vary. Figure 6C shows the linear relation between the value of ΔE^0 and the mean of k^0_1 and k^0_2, for the final parameters of the 100 best fits in this series. The slope is -194 mV/decade, close to the predicted slope of -120 mV/decade that is expected if $\alpha_2 = \alpha_1 = 0.5$ and $k_{01} = k_{02}$; indeed, for the various sets of parameters that give the same peak separation, eqs 8 and 9 can be combined to show that the relation between ΔE^0 and k_0 should be

$$\frac{\mathrm{d}\,\Delta E^0}{\mathrm{d}\,\log_{10} k_0} = -\frac{2.3 \times RT}{\alpha F} \quad (16)$$

The exact relation between the best values of ΔE^0, k_{01}, k_{02}, α_1 and α_2 is further discussed in SI section S11.

The value of the diffusion coefficient affects the positions of the peaks (which depend on $\log(D/k_0^2)$, see e.g. eq 8) and their magnitude (in proportion to $AC(D)^{1/2}$). Since the value of k_0 cannot be determined by fitting, the value of the diffusion coefficient should not be let free in the fitting procedure unless the product AC is fixed to a known value. In all fitting runs discussed in this work, we fixed the values of D and C, and we let free the value of A.

To find out if certain values of ΔE^0 are *not* consistent with the data, we run a systematic exploration by *fixing* 25 values of ΔE^0 in the range -0.8 to 0.2 V, and starting the fits from 60 seeds each time. We discarded the fits for which the product $AC(D)^{1/2}$ is about twice the expected value : they correspond to a situation where the program calculates two separated one-electron irreversible waves, one of which is out of the potential window of the CV. The best fits obtained by fixing ΔE^0 to any value greater than -90 mV are bad (judging by the eye, fig 7A, or from the larger value of the total residual in Panel C). In contrast, an equally good fit is obtained with ΔE^0 fixed to any value lower than -90 mV (fig 7C).

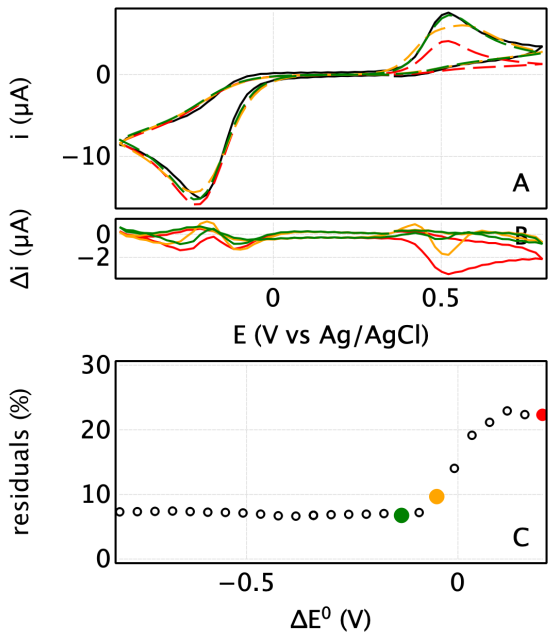

Figure 7. Fitting a CV of $[Ni(BQ)_2(Cl)_2]$ ($\mathbf{1}^{2+}\cdot\mathbf{2Cl}^-$) by forcing the value of ΔE^0.
Panel A: good (green), and bad (orange, red) fits of the 2V/s voltammogram of 1mM $[Ni(BQ)_2(Cl)_2]$ ($\mathbf{1}^{2+}\cdot\mathbf{2Cl}^-$)(same conditions as in 5) obtained after forcing ΔE^0 = -133 (green), -50 (orange) and +200mV (red).
Panel B: Residuals of the fits in panel A
Panel C: Relative residuals of the best fits of the 2V/s CV in figure 5A, forcing ΔE^0 in the range -0.8 to 0.2V and adjusting the other parameters starting for each value of ΔE^0 starting from 60 different seeds defined by $(E^0_1+E^0_2)/2 \in$ [0-0.4V], k_{01} and $k_{02} \in [10^{-8}$-1 cm/s] (on a log scale), AC $\in$ [6-9 10^{-6} mol/cm], $\alpha_1 = 0.5$, $\alpha_2 = 0.3$, $D = 9\ 10^{-6}$ cm^2/s. The plot shows that the fits are equally good for all values of $\Delta E^0 <$ -90 mV.

To test whether ΔE^0 can be measured more accurately by interpreting the dependence of the voltammetric signature on scan rate, we repeated the latest exploration by simultaneously fitting the model to three CVs recorded at 1, 2 and 5 V/s, instead of only one. The same weight was given to all CVs. The results in SI section S8 show that the conclusion is the same as when only one scan rate is considered.

Any value of ΔE^0 lower than the above determined limit would be consistent with the data, but the lower ΔE^0, the larger the value of k_0 that is needed to obtain the same peak separation. Assuming an upper value of k_0 and using eq 14 gives the lower limit of ΔE^0:

$$\Delta E^0_{\min} = -\Delta E^p + \frac{RT}{\alpha F}\left(2 \times 0.78 + \ln \frac{D\alpha F\nu}{k^2_{0\,\max} RT}\right) \quad (17)$$

For the CV in fig 7 for example, ΔE^p = 640 mV at v = 2V/s, and if we assume $k_{0\,max}$ = 1 cm/s (ref [8]), we obtain $\Delta E^0_{\ min} \approx$ -1V.

The effect of dis- and comproportionation

Regarding the particular CV in fig 7A, we examined the effect of including the disproportionation reaction using the same strategy as above. This reaction

$$2\mathrm{I} \underset{k_c}{\overset{k_d}{\rightleftarrows}} \mathrm{O} + \mathrm{R} \quad (18)$$

is bimolecular in both directions, with rate constants k_d and k_c that are related by thermodynamics:

$$\frac{k_d}{k_c} = \exp\left(\frac{-F\,\Delta E^0}{RT}\right) \quad (19)$$

(note that $k_d > k_c$ when the potentials are inverted).

We repeated the exploration of the parameter space by forcing ΔE^0 between -0.8 V and +0.5 V, and forcing the disproportionation rate constant k_d to take values ranging from 10^{-6} to 10^7 cm^3/mol/s,

calculating the corresponding value of k_c using eq. 19, and discarding the combinations of parameters that gave k_c greater than the diffusion limit (10^7 cm^3/mol/s at most). Figure 8 shows a color map of the relative residuals of the 504 resulting best fits (504 = 36 values of ΔE^0 times 14 values of k_d), plotted as a function of ΔE^0 (x-axis) and $\log_{10}(k_d)$ (y-axis). The color code is from green (perfect fit) to red (bad fit), as in fig 7C. The top right corner is blanked, because it corresponds to values of k_c that exceed the diffusion limit.

The lower row of this figure (where k_d is negligibly small) shows the same results as fig 7C: the fit is good (green) irrespective of the value of ΔE^0 below a certain threshold (around -90 mV). Increasing k_d has no strong effect on this threshold, we only see a slight increase in the range of acceptable ΔE^0 values when reaction 18 is very fast.

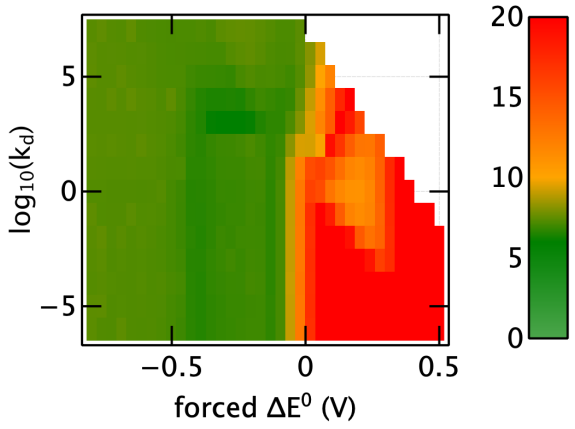

Figure 8 Fitting the CV of [Ni(BQ)$_2$(Cl)$_2$] (**1**$^{2+}$·**2Cl**$^-$) in fig 7A by forcing the values of ΔE^0 and k_d (the disproportionation bimolecular rate constant, in units of cm^3/mol/s). The color map shows the quality of the resulting best fit. The color code is from green (good fit, with relative residuals lower than 7%) to orange (relative residuals ≈ 10%) to red (bad fit), as shown on the color scale on the right. This color scheme is also used in fig 7C. The "best" CVs calculated for ΔE^0 ≈ 0.2 V and k_d ≈ 1 cm^3/mol/s are reasonably good in terms of relative residuals (thus the orange zone), but bad in terms of shape (they show a small oxidative pre-peak resulting from the oxidation of **R** to **I**) that is not observed in experiments.

Generalization

We have focused above on the irreversible case, where the peak separation is large. By discussing the equations of the peak positions we demonstrated that the value of ΔE^0 cannot be determined by fitting, and on a particular example we found that all values of ΔE^0 more negative than -90 mV were consistent with the shape of the voltammograms in figs 5A. Here we wonder if this -90 mV limit is general by examining which values of ΔE^0 can actually be determined from ideal voltammetric responses.

Considering the conditions $k_d = 0$, $k_{01} = k_{02}$ and either $\alpha_1 = \alpha_2 = 0.5$ (top row in fig 9) or $\alpha_1 = 0.5$, $\alpha_2 = 0.4$ (bottom row in fig 9), we run a number of simulations of the voltammetry of the simple two-electron kinetic scheme, using values of $D\alpha Fv/k_0^2RT$ equal to 10^5 (left panels, irreversible limit) and 10^{-10} (right panels, reversible limit) and 36 different "real" values of ΔE^0 ranging from -0.5V to +0.2V. For each simulation, we run a series of fits, *forcing* ΔE^0 to take one of 36 values between -0.5V to +0.2V. Figure 9 shows color maps of the relative residuals of the 5184 resulting best fits (5184 = 2 × 2 × 36 × 36: 2 values of v/k_0^2, times 2 pairs of values of α_1 and α_2, times 36 "real" values of ΔE^0, times 36 "forced" values of ΔE^0), plotted as a function of "ΔE^0 fitted" and "ΔE^0 real". The color code is from green (perfect fit) to red (bad fit), as in fig 7C and 8. Any vertical section of these graphs has the same meaning as fig 7C, except that the four CVs that were fitted were the

results of simulations, rather than the result of experiment. Note that since the CVs fitted in fig 9 are not the same as those in fig 7, the results of the analysis need not be the same.

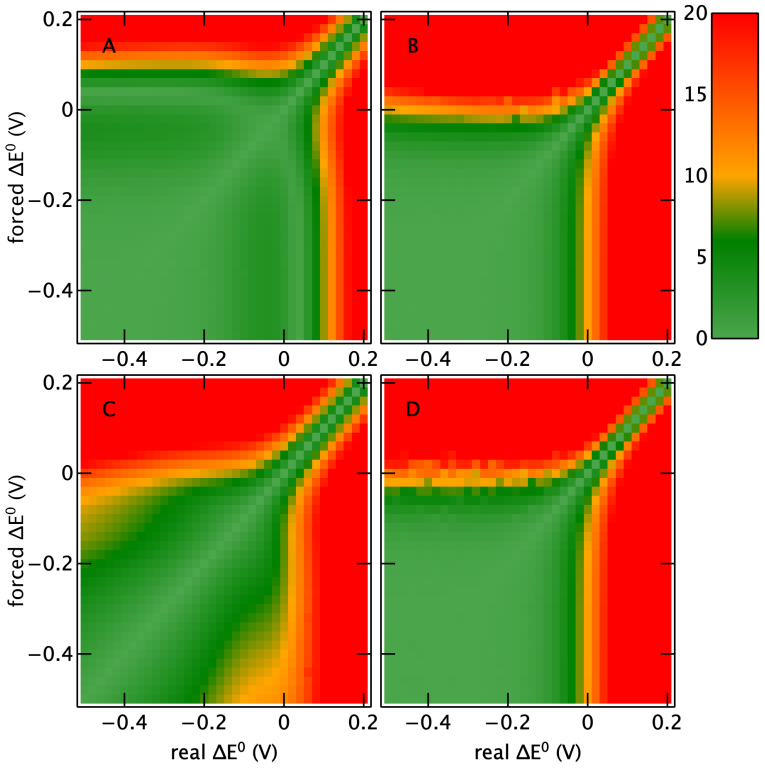

Figure 9. The range of values of ΔE^0 that can be reliably determined by fitting the EE model to a voltammogram. Each plot is a color map of the quality of the best fit obtained by forcing a certain value of ΔE^0 to a voltammogram calculated using a certain "real" value of ΔE^0. The CVs were calculated for $D\alpha Fv/k_0^2RT$ equal to 10^5 (left panels, irreversible situation) and 10^{-10} (right panels, reversible situation), with $k_{01} = k_{02}$ and $\alpha_1 = \alpha_2 = 0.5$ (top), or $k_{01} = k_{02}$ and $\alpha_1 = 0.5$, $\alpha_2 = 0.4$ (bottom). See in fig 2B the shapes of the corresponding CVs. The color code is from green (good fit, with relative residuals lower than 7%) to orange (relative residuals ≈ 10%) to red (bad fit), as shown on the color scale on the right. This color scale is also used in fig 7C and 8.

Unsurprisingly, we observe that when ΔE^0 is positive (when the potentials are not inverted, rightmost part of each panel), the good fits are on the diagonal corresponding to "ΔE^0 fitted" = "ΔE^0 real" ; this means that the real value of ΔE^0 is well determined by the fit. In contrast, when ΔE^0 is negative, any negative value of ΔE^0 is consistent with the data (hence the green, squarish region in the bottom left corner of each panel).

These considerations do not take into account any non-ideality (resulting from high frequency noise, irregular background current, insufficient ohmic drop compensation, heterogeneity etc.) that would distort real data. They set a theoretical limit to the negative values of ΔE^0 that can be measured, but there is no assurance that this precision can be achieved in the analysis of experimental results. Judging from the data in figs 6 and 7, relative deviations of 8 to 10 % correspond visually to very good fits. Using 10% as a threshold (orange in fig 9), we conclude that in the worst case, when the ET is irreversible and $\alpha_1 = \alpha_2 = 0.5$, it is not even possible to discriminate between values of ΔE^0 lower than +100 mV (fig 9A). The case in which the values of α are different is slightly more favorable (the green

region is smaller in panel C than in panel A). If the two values of k_0 and α are very different from one another, it may happen that at a very fast scan rate, our assumption that the 2nd ET is faster than the 1st becomes wrong ; in that case the voltammetry may become more complex, showing more than one peak on each sweep, and, provided the data is of sufficient quality, it maybe possible to analyze it to obtain reliable values of all the parameters (see e.g. ref [34]).

The above analyses shows that in all situations, values of ΔE^0 below a certain limit cannot be discriminated against by fitting, but this limit is not universal: its value depends on the other parameters (the values of k_0 and α) and on the quality of the data (or, equivalently, the fit quality that is considered acceptable).

Discussion

Here we summarize the rules that guide the interpretation of the voltammetry of a two-electron system in the most common case where the voltammograms show only one cathodic and one anodic peak (as in fig 2A) and we explain the implications that have been underlooked in the literature regarding the fitting of voltammograms and the estimation of the extent of potential inversion.

The reversible case (in the limit of slow scan rate) is well known (fig 1C, or red in fig 2A). A two-electron pair of peaks at $E^0_m = (E^0_1+E^0_2)/2$ is expected, with a peak separation $\Delta E^p = E^{pa}-E^{pc}$ that is scan rate independent. If the potential difference is small, e.g. $-80\ mV \lesssim \Delta E^0 \lesssim 80\ mV$, ΔE^0 may be obtained from ΔE^p using a working curve, as in fig 1D. Any deviation from an ideal behavior — the broadening of the signal that would result from slow electron transfer or a dispersion of E^0 values, or a baseline imperfection — is likely to affect the accuracy of the measurement. Moreover, the ideal shape of the signal becomes fully independent of ΔE^0 as ΔE^0 decreases, and very negative values of ΔE^0 ($\Delta E^0 \lesssim -80$ mV) cannot be measured.

At scan rates faster than those defined by eq 12, the voltammetry is irreversible: the oxidative and reductive peaks split as the scan rate increases (as observed in fig 5C and SI figs S8C, S10C), which clearly implies that these peak potentials cannot be equated to the value of any thermodynamic parameter. The peak potentials are given by eqs 8 and 9. These equations do not imply that the peak potentials are close to the E^0 values, because the magnitude of the second term in the right-hand sides of these equations may be large. Furthermore, the sign of these terms may be positive or negative, and an important conclusion here is therefore that the cathodic peak potential may be lower or greater than E^0_1, and the anodic peak potential lower or greater than E^0_2. There is no *range* of scan rates where the peak potentials equal the values of the one-electron reduction potential E^0, and only by chance can E^{pc} or E^{pa} be close to E^0_1 or E^0_2, just like a broken watch gives the right time twice a day.

Equation 14 gives the peak separation $\Delta E^p = E^{pa} - E^{pc}$ for a freely-diffusing two-electron species in the irreversible limit. It is the sum of a thermodynamic contribution $E^0_2 - E^0_1$, which may be large, and a kinetic contribution, which depends on scan rate and may be positive or negative.

A first, obvious consequence is that the peak separation is not a proxy nor an upper or lower limit of $E^0_2 - E^0_1$ ($= -\Delta E^0$).

Second, eq 12 explains the general observation that for systems that show potential inversion, the low scan rate reversible limit is hard to reach. Equation 12 gives the order of magnitude of the scan rate v_{split} above which the peaks separate and shows that for a given value of k_0, the more negative ΔE^0 the smaller this scan rate. Reaching reversibility therefore requires very slow scan rates.[45] It has been considered that when potential inversion occurs, the measured values of k_0 are small because the high reorganization energy related to the structural changes that are coupled to the redox process slows electron transfer[19,29,30,46,47]. In contrast, our analysis shows that the large peak separation that is often observed at moderate scan rates when potential inversion occurs should not be interpreted as evidence that k_0 is particularly small, because this peak separation includes a large thermodynamic contribution (eq 14). Moreover, the values of k_0 can be underestimated by the fitting procedure.

Indeed, the fact that both kinetics and thermodynamics contribute to peak splitting has a very strong implication regarding the fitting of the CVs. The parameters that are adjusted in the fitting procedure are necessarily undetermined to some extent because a very negative ΔE^0 and fast electron transfer may give the same peak splitting as a more positive ΔE^0 combined with slower ET (eq 16). This explains the correlations between the "best" values of k_0 and ΔE^0 that have been observed before (see e.g. table 1 in ref [30]), and it is clearly illustrated by our systematic analysis of the voltammetry of a Ni complex (fig 6). Our conclusion about the indetermination of k_0 and ΔE^0 also stands firm when the analysis consists in fitting a model to a complete voltammogram (therefore taking into account the shape, not just the peak positions), or a set of voltammograms recorded at different scan rates.

To interpret the data in fig 5 (and SI figs S8 and S10), we used the numerical solution of the common two-electron model ("EE"). In contrast to all previous investigations, instead of searching for and reporting a single set of parameters (E^0's, k_0's, D's, α's, etc) that provides a good fit of either one CV or a set of CVs recorded at different scan rates, we used a program that allowed us to fully explore the parameter space, and we wondered whether a single or several sets of parameters actually provide a good fit of the data. Our results clearly show that there is not a unique solution to the fitting problem, irrespective of the number of CVs recorded at different scan rates and simultaneously analyzed. For example the five fits in fig 6 are equally good (judging from the difference between the fit and the data in panel B or the total residues in panel D), but the corresponding 5 best values of ΔE^0 range from -125 to -800 mV, and the k_0 values from 10^{-1} to 10^{-4} cm/s (panel C). Each data point in panels B and C corresponds to one of these good fits. The perfect correlation between the "best" values of k_0 and ΔE^0 (fig 6C) is predicted by eq 16 and results from the additive contributions of thermodynamics and kinetics in the equations that give the peak positions (see also SI section S11). A single best value of ΔE^0 is necessarily found by the fitting procedure if all the other parameters are kept constants, as illustrated in ref [28], but a different result would have been obtained if a different kinetics had been assumed.

There is no *unique* set of parameters (k_0, ΔE^0, etc.) that provides a good fit of the CVs, but we proposed a new method that can be used to determine the *range* of ΔE^0 values that is consistent with a particular data set (either a unique CV, fig 7, or a set of CVs recorded at different scan rates, SI fig S7). It consists in repeatedly fixing ΔE^0 to a certain value, searching for a set of parameters that provide a best fit of the data, and examining how the goodness of this best fit changes as a function of ΔE^0. We found that good fits are only obtained when ΔE^0 is below a certain threshold, which we interpret as the *upper* limit of ΔE^0. Analyzing either one CV or multiple CVs recorded at different scan

rates gives the same results. A *lower limit* of the value of ΔE^0 can also be estimated from eq 17 if a maximal value of k_0 is assumed.

The results in fig 7 illustrate the determination of the upper value of ΔE^0 of -90mV for the $[Ni(BQ)_2(Cl)_2]$ ($\mathbf{1^{2+}\cdot 2Cl^-}$). This value of ΔE^0 is hundreds of mV more positive than minus the peak separation observed in the voltammetry at any scan rate. That potential inversion occurs in the case of that complex is clear from the UV-Vis titration in fig 4, which shows a two-electron conversion with an isosbestic point, but this type of experiment cannot be easily interpreted to estimate the value of ΔE^0. We also used EPR to quantify the amount of intermediate form produced by the partial comproportionation of an equimolar mixture of the oxidized and reduced forms of the complex. No intermediate could be detected, from which, using eq 4, we conclude that $\Delta E^0 \lesssim$ -140 mV ; this result is consistent with (but more restrictive than) the interpretation of the voltammetry.

In an attempt to generalize our conclusions, we examined the results of the fits of simulated (hence ideal) voltammetric data. From fig 9 we concluded that when $k_{01} \approx k_{02}$ and $\alpha_1 \approx \alpha_2 \approx 0.5$, reasonably good fits cannot be used to discriminate negative value of ΔE^0. If the two values of k_0 or the two values of α are so different from one another that the shape of the voltammetry becomes more complex than that seen in fig 5, e.g. with multiple peaks on each sweep, the parameters of the system can actually be determined, at the cost of a thorough analysis as exemplified e.g. in ref [34]. How different the two k_0 values must be for this to be possible depends on ΔE^0, α_1, α_2, the quality of the data and the range of accessible scan rates. It is therefore not possible to draw a general conclusion about which negative values of ΔE^0 can be reliably measured by fitting the voltammetry. However, we have demonstrated that in this sort of analysis, it is crucial to fully explore and define the limits of the *continuous range of parameters* that gives a good fit of the voltammetry, not just consider a single set of "best" parameters. This has not been done before, probably in part because the numerical tools and softwares to achieve this goal were missing.

The pitfalls of non linear fitting should of course be considered in the modeling of any experiment, but the above theoretical analysis explains why the parameters of the simple two-electron model are particularly ill-defined ; this has crucial consequences on the estimation of potential inversion from voltammetric data that have apparently been overlooked before.

Methods

The synthesis and characterization of $\mathbf{1^{2+}\cdot 2Cl^-}$ is described in SI. The structure was deposited to the Cambridge Crystallographic Data Centre (CCDC) under the reference CCDC 2178080.

We used M. Rudolf's "box2" solver,[48] in an in-house simulation program, for integrating the diffusion equations with the electrode boundary conditions. This simulation program was used for the simulations shown in figs 1C, 2A, S1 and S2A. The same simulation program was connected to the open source fitting program QSoas (qsoas.org)[44] to explore the parameter space. The minimization algorithm used in this work was ODRPACK.[49] The relative residuals (%) plotted in figs 6D, 7C, 8, 9, S7D, S9C and S11C are the square root of the weighted average of the square of the difference between the fit and the data divided by the weighted average of the squares of the data, so that they represent an average relative deviation. The simulation program is currently being integrated into the public version of QSoas and will be part of a subsequent release.

Authors contribution

Cheriehan Hessin: Investigation. Jules Schleinitz: Investigation. Nolwenn Le Breton: Investigation Sylvie Choua, Investigation, Supervision. Laurence Grimaud: Writing, Supervision. Vincent Fourmond: Conceptualization, Software, Methodology, Formal analysis, Writing. Marine Desage-El Murr: Conceptualization, Methodology, Writing, Supervision. Christophe Léger: Conceptualization, Investigation, Software, Methodology, Formal analysis, Writing, Supervision

Conflicts of interest

There are no conflicts to declare.

Acknowledgements

The authors thank the reviewers and Andrea Fasano for the critical reading of the manuscript, Dr Lydia Karmazin for the X-ray crystallographic measurements and Dr. Bruno Vincent for DOSY NMR measurements. This work was funded by the CNRS, Aix Marseille University, Strasbourg University, Fondation pour la Recherche en Chimie (FRC), and LabEx CSC (ANR-10-LABX-0026_CSC). The authors are part of the French Network of Bioinorganic Chemistry (www.frenchbic.cnrs.fr).

Supplementary information

Section S1: the voltammetry of a two electron redox system, crossed vs uncrossed cases. Section S2: An example of asymmetric trumpet plot. Section S3: Syntheses. Synthesis of ferrocenium chloride (Fc·Cl). Preparation of $[Ni^{II}(SQ)_2]$ (complex **1**). Synthesis of the aminophenol ligand. Synthesis of $[Ni^{II}(SQ)_2]$ (complex 1). Preparation of $\mathbf{1^{2+}\cdot 2OTf^-}$. Preparation of $\mathbf{1^{2+}\cdot 2Cl^-}$. UV-Vis spectra of the complexes and reactants. Section S4 : EPR spectroscopy experiments. Section S5 : X-ray. characterization of $\mathbf{1^{2+}\cdot 2Cl^-}$. Section S6 : Determination of the diffusion coefficient. Section S7 : Voltammetry (methods). Section S8 : Analysis of the voltammetry of $\mathbf{1^{2+}\cdot 2Cl^-}$ at multiple scan rates. Section S9 : Voltammetry of $\mathbf{1^{2+}\cdot 2Cl^-}$ in CH_2Cl_2+TBACl. Section S10 : Voltammetry of **1** in CH_2Cl_2+TBACl. Section S11 : further discussion of eq 14 and fig 6C. Section S12 : Equations of the peak positions for *surface-confined* (rather than diffusing) two-electron species when potential inversion occurs.

References

(1) Evans, D. H. One-Electron and Two-Electron Transfers in Electrochemistry and Homogeneous Solution Reactions. *Chem. Rev.* **2008**, *108* (7), 2113–2144. doi:10.1021/cr068066l
(2) Lam, K.; Geiger, W. E. Influence of Molecular and Medium Effects on Two-Electron Processes. In *Organic Electrochemistry*; Hammerich, O., Speiser, B., Eds.; CRC Press, 2015; pp 395–431.
(3) Demmer, J. K.; Pal Chowdhury, N.; Selmer, T.; Ermler, U.; Buckel, W. The Semiquinone Swing in the Bifurcating Electron Transferring Flavoprotein/butyryl-CoA Dehydrogenase Complex from Clostridium Difficile. *Nat. Commun.* **2017**, *8* (1), 1577. doi:10.1038/s41467-017-01746-3
(4) Baymann, F.; Schoepp-Cothenet, B.; Duval, S.; Guiral, M.; Brugna, M.; Baffert, C.; Russell, M. J.; Nitschke, W. On the Natural History of Flavin-Based Electron Bifurcation. *Front. Microbiol.* **2018**, *9*, 1357. doi:10.3389/fmicb.2018.01357
(5) Buckel, W.; Thauer, R. K. Flavin-Based Electron Bifurcation, A New Mechanism of Biological

Energy Coupling. *Chem. Rev.* **2018**, *118* (7), 3862–3886. doi:10.1021/acs.chemrev.7b00707
(6) Yuly, J. L.; Lubner, C. E.; Zhang, P.; Beratan, D. N.; Peters, J. W. Electron Bifurcation: Progress and Grand Challenges. *Chem. Commun.* **2019**, *55* (79), 11823–11832. doi:10.1039/C9CC05611D
(7) Yuly, J. L.; Zhang, P.; Ru, X.; Terai, K.; Singh, N.; Beratan, D. N. Efficient and Reversible Electron Bifurcation with Either Normal or Inverted Potentials at the Bifurcating Cofactor. *Chem* **2021**, *7* (7), 1870–1886. doi:10.1016/j.chempr.2021.03.016
(8) Fourmond, V.; Wiedner, E. S.; Shaw, W. J.; Léger, C. Understanding and Design of Bidirectional and Reversible Catalysts of Multielectron, Multistep Reactions. *J. Am. Chem. Soc.* **2019**, *141* (28), 11269–11285. doi:10.1021/jacs.9b04854
(9) Dutta, A.; Appel, A. M.; Shaw, W. J. Designing Electrochemically Reversible H2 Oxidation and Production Catalysts. *Nature Reviews Chemistry* **2018**, *2* (9), 244–252. doi:10.1038/s41570-018-0032-8
(10) Fourmond, V., Plumeré, N., Léger, C. Reversible Catalysis. *Nat. Rev. Chem.* **2021**, *5*, 348–360. doi:10.1038/s41570-021-00268-3
(11) Cunningham, D. W.; Barlow, J. M.; Velasquez, R. S.; Yang, J. Reversible and Selective CO2 to HCO2- Electrocatalysis near the Thermodynamic Potential. *Angew. Chem. Int. Ed Engl.* **2019**. doi:10.1002/anie.201913198
(12) Cunningham, D. W.; Yang, J. Y. Kinetic and Mechanistic Analysis of a Synthetic Reversible CO2/HCO2- Electrocatalyst. *Chem. Commun.* **2020**. doi:10.1039/d0cc05556e
(13) Fourmond, V.; Plumeré, N.; Léger, C. Reversible Catalysis. *Nature Reviews Chemistry* **2021**, *5* (5), 348–360. doi:10.1038/s41570-021-00268-3
(14) Ludwig, K.; Quintanilla, M. G.; Speiser, B.; Stauß, A. Two-Electon-Transfer Redox Systems. *J. Electroanal. Chem.* **2002**, *531* (1), 9–18. doi:10.1016/s0022-0728(02)00996-8
(15) Bonomi, F.; Iametti, S. Redox Titration of Flavoproteins: An Overview. *Methods Mol. Biol.* **2021**, *2280*, 119–133. doi:10.1007/978-1-0716-1286-6_8
(16) Hill, M. G.; Rosenhein, L. D.; Mann, K. R.; Mu, X. H.; Schultz, F. A. IR Spectroelectrochemical Investigation of the Disproportionation of bis(benzenemethanethiolato)octacarbonylditungstate(2-). *Inorg. Chem.* **1992**, *31* (20), 4108–4111. doi:10.1021/ic00046a022
(17) Macías-Ruvalcaba, N. A.; Evans, D. H. Studies of Potential Inversion in the Electrochemical Reduction of 11,11,12,12-Tetracyano-9,10-Anthraquinodimethane and 2,3,5,6-Tetramethyl-7,7,8,8-Tetracyano-1,4-Benzoquinodimethane. *J. Phys. Chem. B* **2006**, *110* (10), 5155–5160. doi:10.1021/jp0573893
(18) Myers, R. L.; Shain, I. Determination of E20 - E10, for Overlapping Waves in Stationary Electrode Polarography. *Anal. Chem.* **1969**, *41* (7), 980–980. doi:10.1021/ac60276a011
(19) Bellec, N.; Boubekeur, K.; Carlier, R.; Hapiot, P.; Lorcy, D.; Tallec, A. Controlling the Conformation Changes Associated to Electron Transfer Steps through Chemical Substitution: Intriguing Redox Behavior of Substituted Vinylogous TTF. *J. Phys. Chem. A* **2000**, *104* (43), 9750–9759. doi:10.1021/jp001326x
(20) Plichon, V.; Laviron, E. Theoretical Study of a Two-Step Reversible Electrochemical Reaction Associated with Irreversible Chemical Reactions in Thin Layer Linear Potential Sweep Voltammetry. *J. Electroanal. Chem. Interfacial Electrochem.* **1976**, *71* (2), 143–156. doi:10.1016/S0022-0728(76)80030-7
(21) Heering, H. A.; Weiner, J. H.; Armstrong, F. A. Direct Detection and Measurement of Electron Relays in a Multicentered Enzyme: Voltammetry of Electrode-Surface Films of E. Coli Fumarate Reductase, an Iron−Sulfur Flavoprotein. *J. Am. Chem. Soc.* **1997**, *119* (48), 11628–11638. doi:10.1021/ja9723242
(22) Richardson, D. E.; Taube, H. Determination of E20-E10 in Multistep Charge Transfer by Stationary-Electrode Pulse and Cyclic Voltammetry: Application to Binuclear Ruthenium Ammines. *Inorg. Chem.* **1981**, *20* (4), 1278–1285. doi:10.1021/ic50218a062
(23) Nomrowski, J.; Wenger, O. S. Exploiting Potential Inversion for Photoinduced Multielectron

Transfer and Accumulation of Redox Equivalents in a Molecular Heptad. *J. Am. Chem. Soc.* **2018**, *140* (16), 5343–5346. doi:10.1021/jacs.8b02443
(24) Wise, C. E.; Ledinina, A. E.; Mulder, D. W.; Chou, K. J.; Peters, J. W.; King, P. W.; Lubner, C. E. An Uncharacteristically Low-Potential Flavin Governs the Energy Landscape of Electron Bifurcation. *Proc. Natl. Acad. Sci. U. S. A.* **2022**, *119* (12), e2117882119. doi:10.1073/pnas.2117882119
(25) Hapiot, P.; Kispert, L. D.; Konovalov, V. V.; Savéant, J. M. Single Two-Electron Transfers vs Successive One-Electron Transfers in Polyconjugated Systems Illustrated by the Electrochemical Oxidation and Reduction of Carotenoids. *J. Am. Chem. Soc.* **2001**, *123* (27), 6669–6677. doi:10.1021/ja0106063
(26) Hudson, J. M.; Heffron, K.; Kotlyar, V.; Sher, Y.; Maklashina, E.; Cecchini, G.; Armstrong, F. A. Electron Transfer and Catalytic Control by the Iron-Sulfur Clusters in a Respiratory Enzyme, E. Coli Fumarate Reductase. *J. Am. Chem. Soc.* **2005**, *127* (19), 6977–6989. doi:10.1021/ja043404q
(27) Smith, W. H.; Bard, A. J. Electrochemical Reactions of Organic Compounds in Liquid Ammonia. *J. Electroanal. Chem. Interfacial Electrochem.* **1977**, *76* (1), 19–26. doi:10.1016/s0022-0728(77)80003-x
(28) Kraiya, C.; Evans, D. H. Investigation of Potential Inversion in the Reduction of 9,10-Dinitroanthracene and 3,6-Dinitrodurene. *J. Electroanal. Chem.* **2004**, *565* (1), 29–35. doi:10.1016/j.jelechem.2003.09.024
(29) Hu, K.; Evans, D. H. Electron-Transfer Reactions with Significant Inner Reorganization Energies. Two-Electron Oxidation of Derivatives of 1,4-Bis(dialkylamino)-1,3-Butadiene. *J. Phys. Chem.* **1996**, *100* (8), 3030–3036. doi:10.1021/jp951909k
(30) Hu, K.; Evans, D. H. Electron-Transfer Reactions Accompanied by Substantial Structural Changes: Oxidation of 9,10-Bis(dimethylamino)anthracene and 3,6-Bis(dimethylamino)durene. *J. Electroanal. Chem.* **1997**, *423* (1), 29–35. doi:10.1016/S0022-0728(96)04880-2
(31) Elgrishi, N.; Rountree, K. J.; McCarthy, B. D.; Rountree, E. S.; Eisenhart, T. T.; Dempsey, J. L. A Practical Beginner's Guide to Cyclic Voltammetry. *J. Chem. Educ.* **2018**, *95* (2), 197–206. doi:10.1021/acs.jchemed.7b00361
(32) Bard, A. J.; Faulkner, L. R. *Electrochemical Methods: Fundamentals and Applications*; Wiley, 2000.
(33) Henstridge, M. C.; Laborda, E.; Rees, N. V.; Compton, R. G. Marcus–Hush–Chidsey Theory of Electron Transfer Applied to Voltammetry: A Review. *Electrochim. Acta* **2012**, *84*, 12–20. doi:10.1016/j.electacta.2011.10.026
(34) Pierce, D. T.; Geiger, W. E. Electrochemical Kinetic Discrimination of the Single-Electron-Transfer Events of a Two-Electron-Transfer Reaction: Cyclic Voltammetry of the Reduction of the Bis(hexamethylbenzene)ruthenium Dication. *J. Am. Chem. Soc.* **1992**, *114* (15), 6063–6073. doi:10.1021/ja00041a026
(35) Laviron, E. Electrochemical Reactions with Protonations at Equilibrium: Part VII. The 2 E, 1H+ Reaction (six-Member Fence Scheme) for a Surface or for a Heterogeneous Reaction in the Absence of Disproportionation or Dimerization. *J. Electroanal. Chem. Interfacial Electrochem.* **1983**, *146* (1), 1–13. doi:10.1016/S0022-0728(83)80109-0
(36) Gruhn, N. E.; Macías-Ruvalcaba, N. A.; Evans, D. H. Studies of the Inner Reorganization Energies of the Cation Radicals of 1,4-Bis(dimethylamino)benzene, 9,10-Bis(dimethylamino)anthracene, and 3,6-Bis(dimethylamino)durene by Photoelectron Spectroscopy and Reinterpretation of the Mechanism of the Electrochemical Oxidation of the Parent Diamines. *J. Phys. Chem. A* **2006**, *110* (17), 5650–5655. doi:10.1021/jp060453b
(37) Gruhn, N. E.; Macías-Ruvalcaba, N. A.; Evans, D. H. Studies of Potential Inversion in an Extended Tetrathiafulvalene. *Langmuir* **2006**, *22* (25), 10683–10688. doi:10.1021/la0611460
(38) Ryan, M. D. The Effect of Slow Two-Electron Transfers and Disproportionation on Cyclic Voltammograms. *J. Electrochem. Soc.* **1978**, *125* (4), 547. doi:10.1149/1.2131496
(39) Hinkelmann, K.; Heinze, J. Analysis of "two-Electron" Transfer Processes by Cyclic Voltammetry. *Ber. Bunsenges. Phys. Chem.* **1987**, *91* (3), 243–249. doi:10.1002/bbpc.19870910315

(40) Nicholson, R. S.; Shain, I. Theory of Stationary Electrode Polarography. Single Scan and Cyclic Methods Applied to Reversible, Irreversible, and Kinetic Systems. *Anal. Chem.* **1964**, *36* (4), 706–723. doi:10.1021/ac60210a007
(41) Christopoulos, A.; Lew, M. J. Beyond Eyeballing: Fitting Models to Experimental Data. *Crit. Rev. Biochem. Mol. Biol.* **2000**, *35* (5), 359–391. doi:10.1080/10409230091169212
(42) Broere, D. L. J.; Plessius, R.; van der Vlugt, J. I. New Avenues for Ligand-Mediated Processes – Expanding Metal Reactivity by the Use of Redox-Active Catechol, O-Aminophenol and O-Phenylenediamine Ligands. *Chem. Soc. Rev.* **2015**, *44* (19), 6886–6915. doi:10.1039/C5CS00161G
(43) Chaudhuri, P.; Verani, C. N.; Bill, E.; Bothe, E.; Weyhermüller, T.; Wieghardt, K. Electronic Structure of Bis(o-Iminobenzosemiquinonato)metal Complexes (Cu, Ni, Pd). The Art of Establishing Physical Oxidation States in Transition-Metal Complexes Containing Radical Ligands. *J. Am. Chem. Soc.* **2001**, *123* (10), 2213–2223. doi:10.1021/ja003831d
(44) Fourmond, V. QSoas: A Versatile Software for Data Analysis. *Anal. Chem.* **2016**, *88* (10), 5050–5052. doi:10.1021/acs.analchem.6b00224
(45) Evans, D. H.; Juusola, P.; Minkkinen, P.; Olsen, C.; Søtofte, I.; Francis, G.; Szunyog, J.; Langstrom, B. The Kinetic Burden of Potential Inversion in Two-Electron Electrochemical Reactions. *Acta Chem. Scand.* **1998**, *52* (2), 194–197. doi:10.3891/acta.chem.scand.52-0194
(46) Evans, D. H.; Hu, K. Inverted Potentials in Two-Electron Processes in Organic Electrochemistry. *J. Chem. Soc. Faraday Trans.* **1996**, *92* (20), 3983–3990. doi:10.1039/FT9969203983
(47) Speiser, B.; Würde, M.; Maichle-Mössmer, C. Electrochemical Oxidation of Hexakis(dimethylamino)benzene. *Chemistry* **1998**, *4* (2), 222–233. doi:10.1002/(sici)1521-3765(19980210)4:2<222::aid-chem222>3.0.co;2-h
(48) Rudolph, M. Attaining Exponential Convergence for the Flux Error with Second- and Fourth-Order Accurate Finite-Difference Equations. II. Application to Systems Comprising First-Order Chemical Reactions. *J. Comput. Chem.* **2005**, *26* (6), 633–641. doi:10.1002/jcc.20201
(49) Boggs, P. T.; Donaldson, J. R.; Byrd, R. h.; Schnabel, R. B. Algorithm 676: ODRPACK: Software for Weighted Orthogonal Distance Regression. *ACM Trans. Math. Softw.* **1989**, *15* (4), 348–364. doi:10.1145/76909.76913

Assessing the extent of potential inversion by cyclic voltammetry: theory, pitfalls, and application to a nickel complex with redox-active iminosemiquinone ligands - Supplementary Information

Cheriehan Hessin (a), Jules Schleinitz (b), Nolwenn Le Breton (a), Sylvie Choua (a), Laurence Grimaud (b), Vincent Fourmond (c), Marine Desage-El Murr *(a), Christophe Léger *(c)

(a) Université de Strasbourg, Institut de Chimie, UMR CNRS 7177, 67000 Strasbourg, France

(b) Laboratoire des Biomolécules, Département de Chimie, Sorbonne Université, École Normale Supérieure, PSL University, CNRS, 75005 Paris, France

(c) Laboratoire de Bioénergétique et Ingénierie des Protéines. CNRS, Aix Marseille Université, 13009 Marseille, France

Section S1: the voltammetry of a two electron redox system, crossed vs uncrossed cases

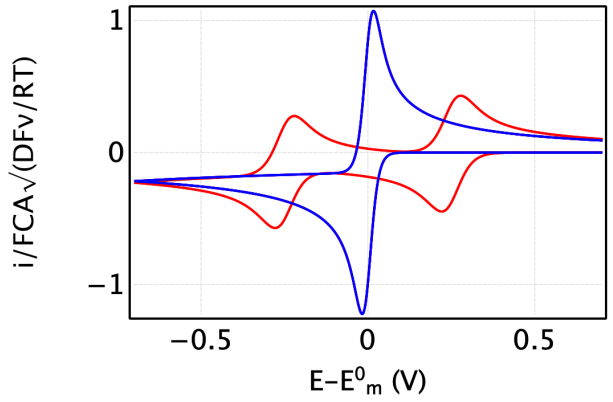

Figure S1. Illustration of the shapes of *reversible* voltammograms of diffusive two-electron species, when the potentials are inverted (blue, $\Delta E^0 << 0$) or uncrossed (red, here with E^0_1=0.25V and E^0_2=-0.25V vs E^0_m)

Section S2: An example of asymmetric trumpet plot

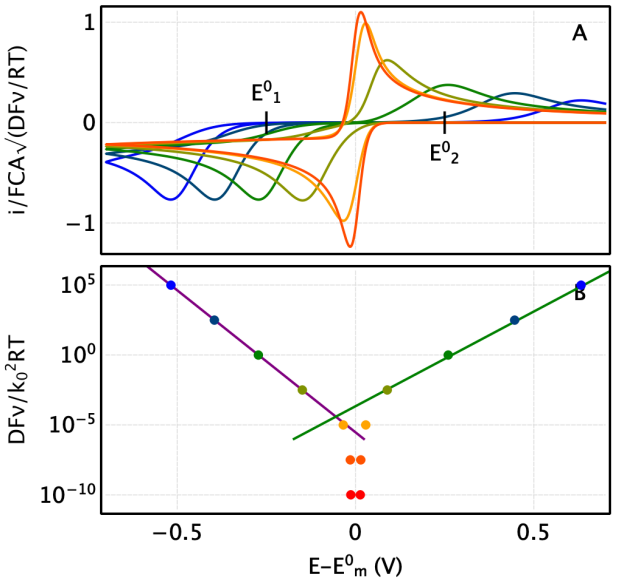

Figure S2: Voltammetric signatures of a diffusing redox molecule that undergoes cooperative two-electron transfer. Same as main text figure 2, but calculated with $\alpha_1 = \alpha_2 = 0.6$, to show an example of a dissymmetrical trumpet plot.

Section S3: syntheses

General information

All reactions were carried out under argon atmosphere using standard Schlenk techniques in oven dried glassware. Reagent grade dichloromethane (CH_2Cl_2) and toluene were purified using a solvent purification system. All starting materials were purchased from commercially available sources (TCI Chemicals, SigmaAldrich, Alfa Aesar, Acros Organics) and used without any further purification. High-resolution mass spectrometry (HRMS) was performed by ESI mass spectrometers MicroTOF(I) and MicroTOF(II) focus (BRUKER, Germany). UV-Vis data were collected using AGILENT Cary 60 UV-Vis Spectrometer at room temperature. Wavelengths (λ) are given in nanometer (nm) and molar extinction coefficients (ε) are given in $M^{-1}.cm^{-1}$. EPR spectra were recorded on an EMXplus spectrometer (Bruker Biospin GmbH) operating at X-band (9.8 GHz), equipped with a high sensitivity resonator (4119HS-W1, Bruker) using 1 mW microwave power, 0.4 mT modulation amplitude, a sweep time of 120 s and 2500 points for a single scan. Powder X-ray diffraction (PXRD) was performed on Bruker D8 Advance with X-ray source by anticathode of copper giving photons with a wavelength of $1.54x10^{-10}$ m. The crystals were placed in oil, and a single crystal was selected, mounted on a glass fiber and placed in a low-temperature N_2 stream. X-Ray diffraction data collection were measured by either 4-circles Bruker PHOTON III diffractometer equipped with two micro-sources IμS Mo and IμS Diamond Cu and with an Oxford Cryosystem 800 for low temperature measurements or 4-circles Bruker APEX II DUO IμS Kappa-CCD diffractometer equipped with two sources (Mo sealed tube and Cu micro-source) and with an Oxford Cryosystem 700 liquid N_2 device for low temperature measurements. The cell parameters were determined in APEX3 software. The structure was solved using the program SHELXT-2014. The refinement and all further calculations were carried out using SHELXL-2018. The H-atoms were included in calculated positions and treated as riding atoms using SHELXL default parameters. The non-H atoms were refined anisotropically, using weighted full-matrix least-squares on F2. A semi-empirical absorption correction was applied using SADABS in APEX3. The structure of $1^{2+}\cdot 2Cl^-$ was deposited to the Cambridge Crystallographic Data Centre (CCDC) under the reference CCDC 2178080.

Synthesis of ferrocenium chloride (Fc·Cl)

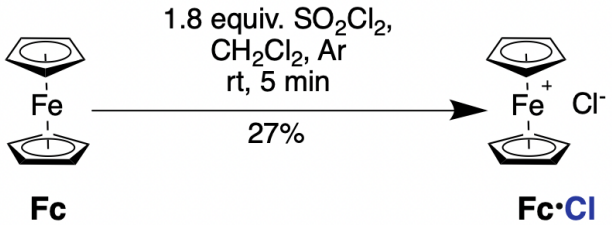

Ferrocenium chloride (**Fc·Cl**) was synthesized according to a literature procedure.[1] To a solution of ferrocene **Fc** (10.0 g, 53.8 mmol) in CH_2Cl_2 (60 mL), SO_2Cl_2 (8 mL, 99 mmol) was added dropwise. The orange reaction mixture turned dark blue, and the blue precipitate was filtered and washed three times with 25 mL of diethyl ether. 100 mL of diethyl ether were added to the filtrated and the blue

[1] Adams, J. J.; Arulsamy, N.; Sullivan, B. P.; Roddick, D. M.; Neuberger, A.; Schmehl, R. H. Homoleptic Tris-Diphosphine Re(I) and Re(II) Complexes and Re(II) Photophysics and Photochemistry. *Inorg. Chem.* **2015**, *54* (23), 11136–11149. doi: 10.1021/acs.inorgchem.5b01395.

precipitate was again filtered. The final product **Fc·Cl** was obtained as a green-blue solid. Yield = 27% (3.26 g, 14.7 mmol).

Preparation of $Ni^{II}(SQ)_2$ (complex 1)

Synthesis of the aminophenol ligand

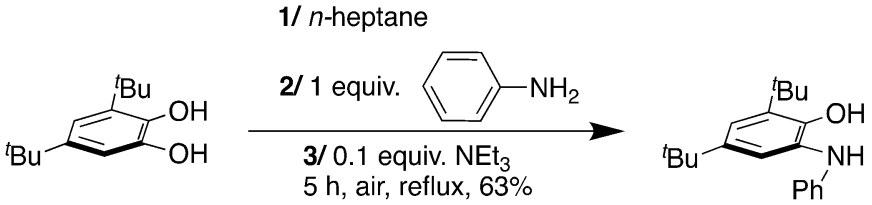

The aminophenol ligand was synthesized according to a literature procedure.[2] To a suspension of catechol (10 g, 44.98 mmol, 1 equiv.) in *n*-heptane (53 mL), was added 4.1 mL of aniline (44.98 mmol, 1.0 equiv.) then 0.64 mL of NEt_3 (4.498 mmol, 0.1 equiv.). The dark brown solution was heated to reflux under air for 5 h. It was then allowed to return to rt and was stored at 4°C overnight. Big slightly pink-orange crystals were obtained, filtered and dried under vacuum. Yield = 63% (8.43 g, 28.34 mmol). Characterization data for this molecule were similar to those reported in the literature.

Synthesis of $Ni^{II}(SQ)_2$ (complex 1)

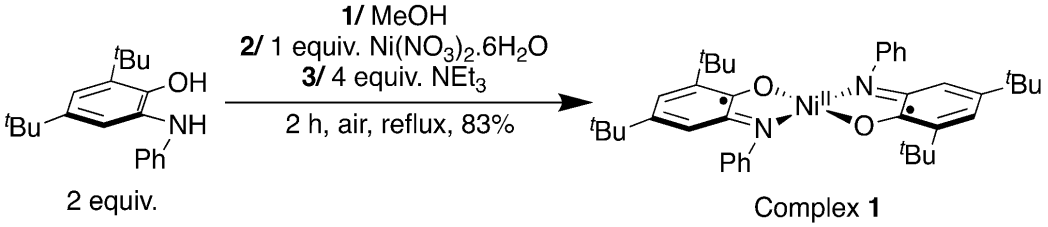

Complex **1** was synthesized according to a literature procedure.[2] To a solution of the aminophenol ligand (2 g, 6.72 mmol, 2 equiv.) in MeOH (88 mL), was added $Ni(NO_3)_2.6H_2O$ (977.7 mg, 3.362 mmol, 1.0 equiv.) then Et_3N (1.87 mL, 13.45 mmol, 4 equiv.). The resulting solution was heated to reflux under air for 1 h. Upon cooling, a dark green precipitate formed. The precipitate was filtered and washed with MeOH to yield a green powder. Yield= 83% (1.8 g, 2.79 mmol). The complex is stored at 4°C. It can be recrystallized by dissolving it in Et_2O and layering that solution on top of a MeOH solution (Et_2O:MeOH, 3:1) mixture. Characterization data of this complex were similar to those reported in the literature.

Preparation of $1^{2+}\cdot 2OTf^-$

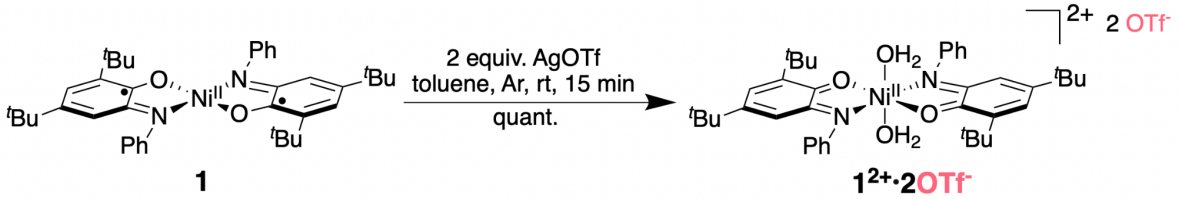

[2] Chaudhuri, P.; Verani, C. N.; Bill, E.; Bothe, E.; Weyhermüller, T.; Wieghardt, K. Electronic Structure of Bis(*o*-Iminobenzosemiquinonato)Metal Complexes (Cu, Ni, Pd). The Art of Establishing Physical Oxidation States in Transition-Metal Complexes Containing Radical Ligands. *J. Am. Chem. Soc.* **2001**, *123* (10), 2213–2223. doi: 10.1021/ja003831d.

Complex **1** (551 mg, 0.848 mmol, 1.0 equiv.) and AgOTf (435.9 mg, 1.697 mmol, 2.0 equiv.) were placed in a Schlenk tube (three Ar/vacuum cycles), followed by 100 mL of toluene (anhydrous under argon). The green solution quickly turned brown-orange and was left to stir for 15 min. The reaction can be monitored by UV-Visible spectroscopy by following the disappearance of the starting material. The brown reaction mixture was then filtered and concentrated under reduced pressure to yield $\mathbf{1^{2+}\cdot 2OTf^-}$ quantitatively as a brown solid. The complex is stored at 4°C. Red prismatic monocrystals were obtained from slow evaporation of CH_2Cl_2 at rt or by layering CH_2Cl_2/Et_2O at 4°C. H atoms and two CH_2Cl_2 molecules were omitted for clarity.

MW ($C_{42}H_{54}F_6N_2NiO_{10}S_2$): 983.70 g/mol.
EPR (CH_2Cl_2): X-band silent (S=1).
HRMS (ESI): (*m/z*) calcd for $C_{40}H_{50}N_2NiO_2$ 324.1607, found 324.1628 $[M]^{2+}$.
CHN analysis: calcd for $\mathbf{1^{2+}\cdot 2OTf^-}$: 51.28 C%, 5.53 H%, 2.85 N%, found 51.14 C%, 5.63 H%, 2.74 N%.
UV-Vis [CH_2Cl_2; λ, nm (ε $M^{-1}.cm^{-1}$)]: 493 (6855 $M^{-1}.cm^{-1}$).

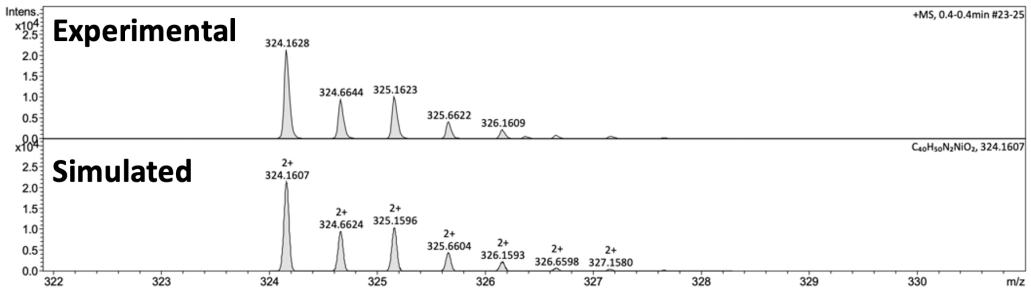

Experimental and simulated HRMS spectrum of $\mathbf{1^{2+}\cdot 2OTf^-}$.

Preparation of $\mathbf{1^{2+}\cdot 2Cl^-}$

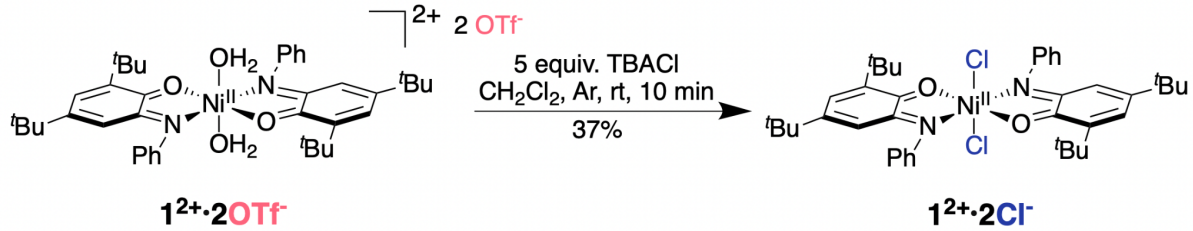

$\mathbf{1^{2+}\cdot 2OTf^-}$ $\mathbf{1^{2+}\cdot 2Cl^-}$

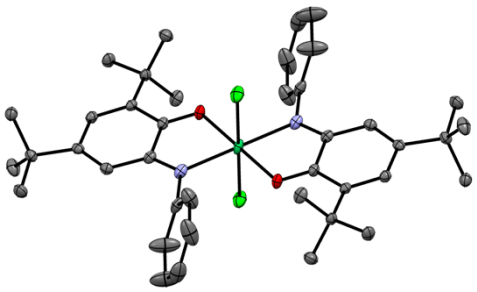

$\mathbf{1^{2+}\cdot 2OTf^-}$ (53.6 mg, 0.054 mmol, 1.0 equiv.,) and TBACl (75.7 mg, 0.272 mmol, 5.0 equiv.) were placed in a Schlenk tube (three Ar/vacuum cycles), followed by 10 mL of CH_2Cl_2 (anhydrous under argon). The mixture was left to stir for 10 min. The brown reaction mixture was then filtered and concentrated under reduced pressure. The solid was washed with water to remove excess TBACl, and toluene or acetone to remove TBAOTf and yield 13.9 mg of a brown-orange solid. Yield = 37%.

Orange plates monocrystals were obtained from layering MeOH/Et_2O and kept at 4°C. $\mathbf{1^{2+}\cdot 2Cl^-}$ is stored at 4°C. CAUTION ! The complex gets reduced during the recrystallization process, the reduced form can be removed by trituration in MeOH.

MW ($C_{40}H_{50}Cl_2N_2NiO_2$): 720.45 g/mol.
EPR (CH_2Cl_2): X-band silent (S=1).
HRMS (ESI): (*m/z*) calcd for $C_{40}H_{50}ClN_2NiO_2$ 683.2909, found 683.2903 $[M]^+$.
CHN analysis: calcd for $1^{2+}\cdot 2Cl^-\cdot 0.2\ CH_2Cl_2$ 65.48 C%, 6.89 H%, 3.80 N%, found 65.16 C%, 6.97 H%, 3.87 N%.
UV-Vis [CH_2Cl_2; λ, nm (ε $M^{-1}.cm^{-1}$)]: 448 (6543 $M^{-1}.cm^{-1}$), 350 (7591 $M^{-1}.cm^{-1}$).

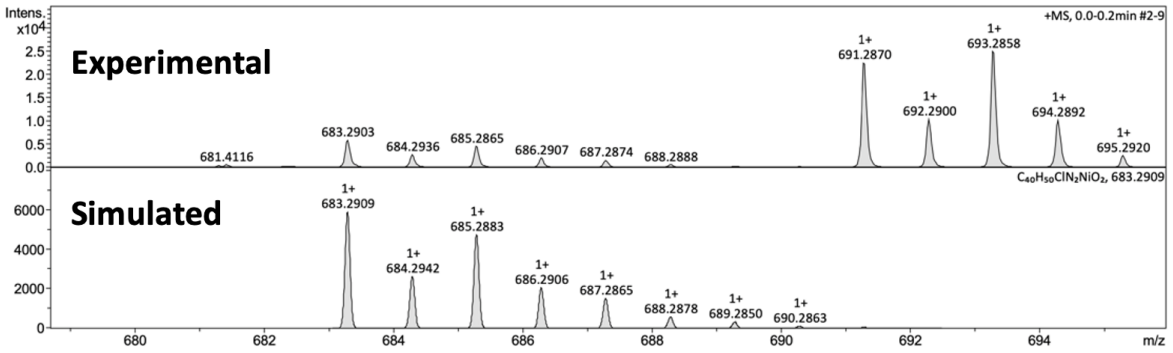

Experimental and simulated HRMS spectrum of $\mathbf{1^{2+}\cdot 2Cl^-}$.

UV-Vis spectra of the complexes and reactants

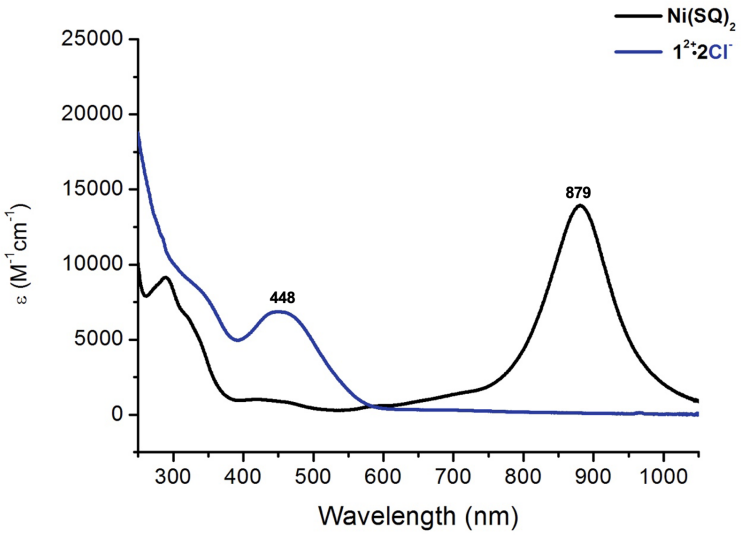

Figure S3. UV-vis absorption spectrum of complex **1** (26 µM) in degassed CH_2Cl_2 (λ = 879 nm, ε = 13934 $M^{-1}.cm^{-1}$; λ = 289 nm, ε = 9145 $M^{-1}.cm^{-1}$) and $\mathbf{1^{2+}\cdot 2Cl^-}$ (50 µM) in degassed CH_2Cl_2 (λ = 448 nm, ε = 6543 $M^{-1}.cm^{-1}$, λ = 350 nm, ε = 7591 $M^{-1}.cm^{-1}$).

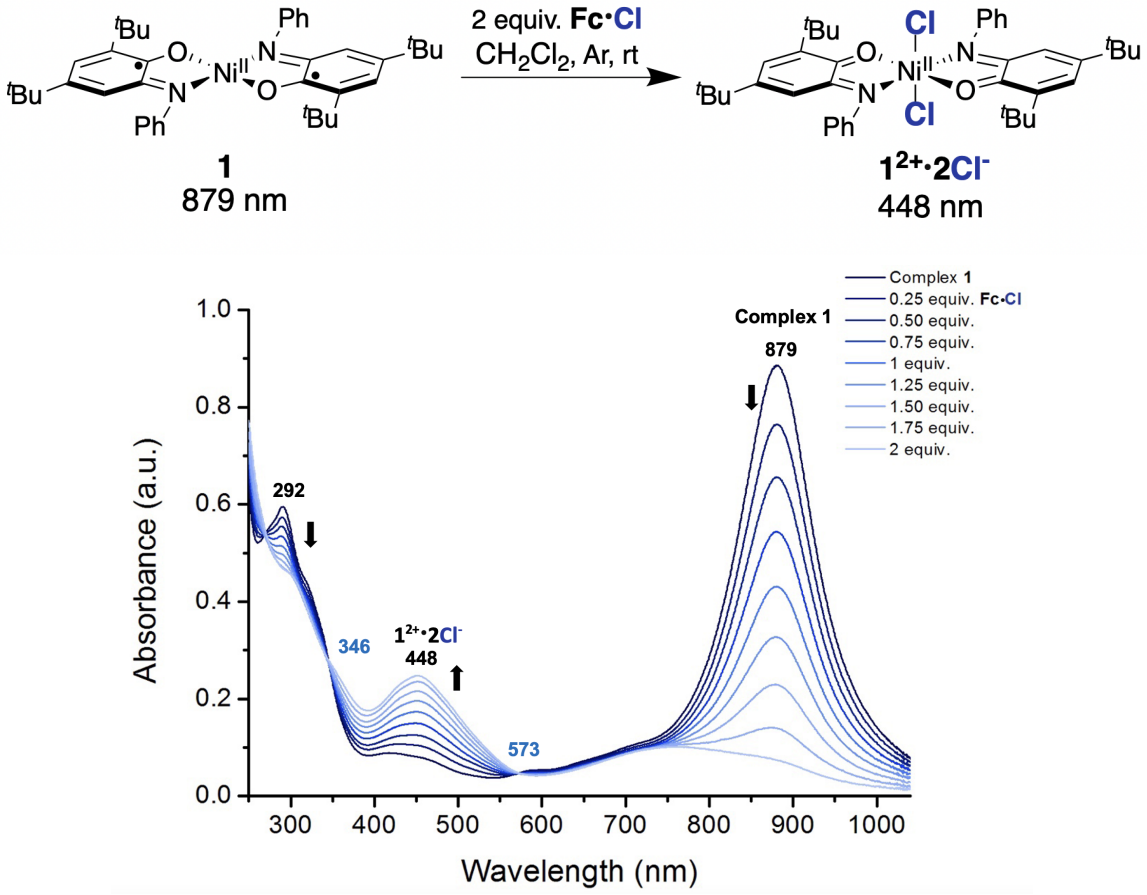

Figure S4. *In-situ* UV-vis absorption spectrophotometric titration of complex **1** (26 µM) with increasing amounts of **Fc·Cl** (0 ⟶ 2 equiv.) in degassed CH_2Cl_2.

Section S4 : EPR spectroscopy experiments

For the following experiments, the fully oxidized form **1**$^{2+}$**·2OTf**$^{-}$ was synthesized using 1 equiv. of complex **1** and 1 equiv. of AgOTf instead of 2 equiv. of AgOTf, to make sure that there were no traces of the oxidant AgOTf left. This reaction yielded 0.5 equiv. of **1**$^{2+}$**·2OTf**$^{-}$, Ag(0), and 0.5 equiv. of complex **1** remained unreacted. Ag(0) was removed by filtration of the crude product and the unreacted Ni(SQ)$_2$ **1** was removed by trituration in MeOH. Complex **1**$^{2+}$**·2Cl**$^{-}$ was synthesized using the above batch of **1**$^{2+}$**·2OTf**$^{-}$ and using the protocol described in section 3.

Two solutions of 1 mM of complex **1** and 1 mM of **1**$^{2+}$**·2Cl**$^{-}$ containing 0.1 M of $TBABF_4$ each were prepared under Ar and in degassed CH_2Cl_2 using a Schlenk line. The two solutions were then placed in an anaerobic glovebox and 1 mL of 1 mM of **1** and 1 mL of 1 mM of **1**$^{2+}$**·2Cl**$^{-}$ were mixed in another glassware. The final solution was placed inside a 100 µL capillary (Hirschmann) and was probed by EPR. No signal was detected at rt.

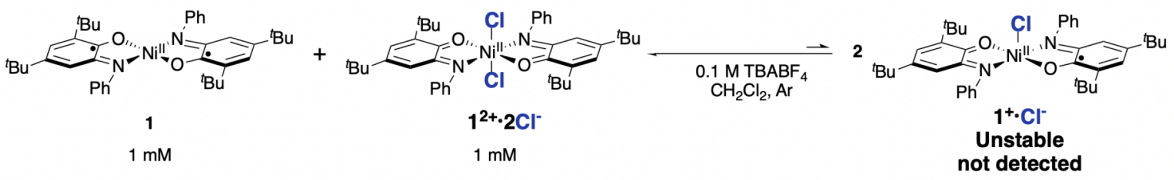

The absence of EPR signals signifies that the concentration of the generated intermediate species $\mathbf{1^{+}\cdot Cl^{-}}$ is below detection by EPR, meaning that the concentration of the generated species is < 1 µM.

Section S5 : X-ray structure of $\mathbf{1^{2+}\cdot 2Cl^{-}}$

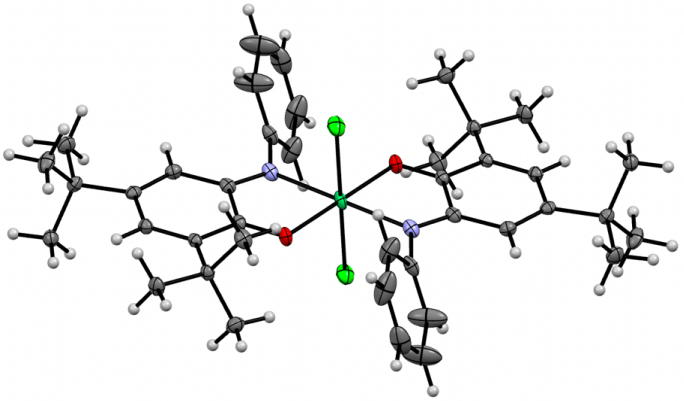

Figure S5. Thermal ellipsoid representation (50% probability) of $\mathbf{1^{2+}\cdot 2Cl^{-}}$.

Table S1. Crystallographic parameters for $\mathbf{1^{2+}\cdot 2Cl^{-}}$.

Product	**Complex $\mathbf{1^{2+}\cdot 2Cl^{-}}$**	
Empirical formula	$C_{40}H_{50}Cl_2N_2NiO_2$	
Formula weight	720.43 g/mol	
Temperature	120(2) K	
Wavelength	0.71073 Å	
Crystal system	monoclinic	
Space group	*P 21/c*	
Unit cell dimensions	*a* = 9.1619(3) Å	α = 90°
	b = 12.4122(4) Å	β = 101.7950(10)°
	c = 16.6415(6) Å	γ = 90°
Volume	1852.50(11) Å^3	
Z	2	
Density (calculated)	1.292 Mg/m^3	
Absorption coefficient	0.704 mm^{-1}	
F(000)	764	
Crystal size	0.200 mm x 0.150 mm x 0.120 mm	
Theta range for data collection	2.271 to 27.905°	
Index ranges	-12<=h<=12; -16<=k<=16; -21<=l<=21	
Reflections collected	52445	
Independent reflections	4419 [*R*(int) = 0.0559]	
Reflections observed (>2sigma)	3867	
Data / restraints / parameters	4419 / 0 / 220	
Goodness-of-fit on *F*2	1.089	

Final R indices [*I*>2sigma(*I*)]	*R*1 = 0.0364 *wR*2 = 0.0907
***R* indices (all data)**	*R*1 = 0.0441 *wR*2 = 0.0960

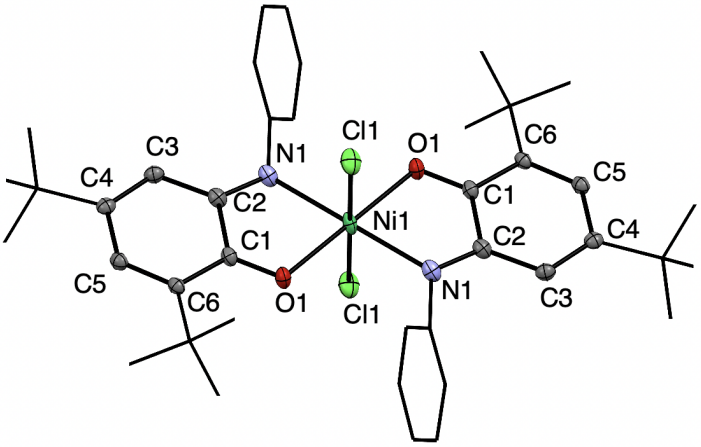

Table S2. Bond distances (Å) for $\mathbf{1^{2+}\cdot 2Cl^{-}}$.

Ni-N1	2.0688(17)	**O1-C1**	1.235(2)	**C1-C2**	1.511(3)	**C1-C6**	1.466(2)	**C6-C5**	1.350(3)
Ni-O1	2.0455(13)	**N1-C2**	1.297(2)	**C4-C5**	1.471(3)	**C2-C3**	1.440(3)	**C3-C4**	1.353(3)
Ni-Cl1	2.3785(5)								

Table S3. Selected angles (º) for $\mathbf{1^{2+}\cdot 2Cl^{-}}$.

Cl1-Ni1-O1	92.96(4)	**O1-Ni1-N1**	101.60(6)
Cl1-Ni1-N1	93.83(5)	**O1-Ni1-N1**	78.39(6)
Cl1-Ni1-Cl1	180.0	**O1-Ni1-O1**	180.0

Section S6 : Determination of the diffusion coefficient

The diffusion coefficient of **1** was determined to be 8.96 x 10^{-10} m^2/s using DOSY NMR. The fit was done using the following equation where ***I*** is the observed intensity, I_0 the reference intensity, ***D*** the diffusion coefficient, γ the gyromagnetic ratio of the observed nucleus, **g** the gradient strength, **δ** the length of the gradient, Δ the diffusion time and τ the time between the bipolar gradient:

$$I = I_0 \, e^{-D\gamma^2 g^2 \delta^2 (\Delta - \delta/3 - \tau/2)}$$

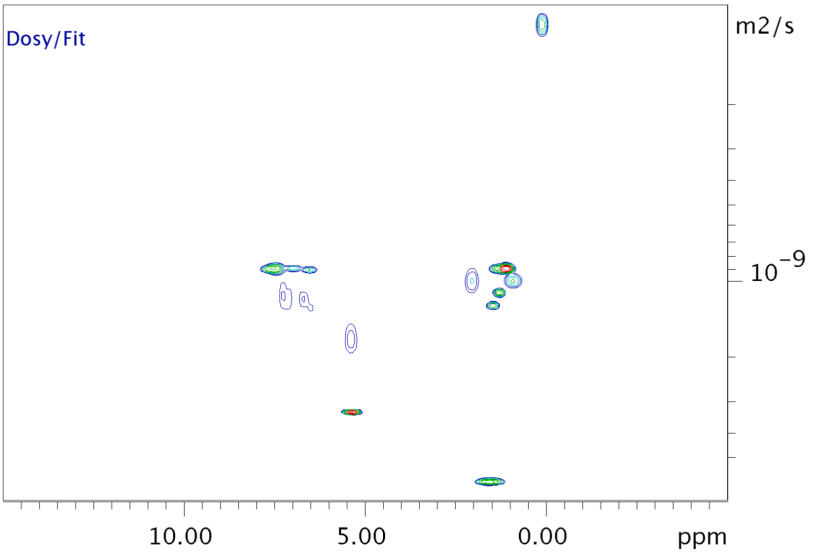

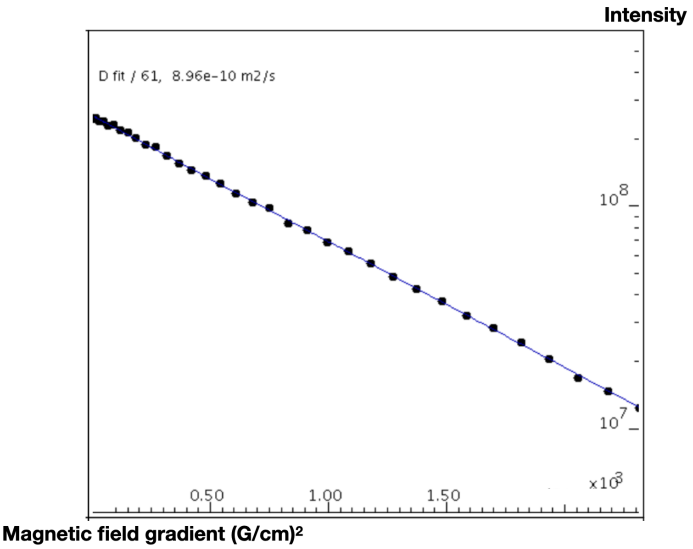

Figure S6. DOSY NMR of complex **1** ($CDCl_3$, 600 MHz) and diffusion coefficient fit plot.

Section S7 : Voltammetry (methods)

All electrochemical experiments were performed under argon flow in a three-electrode cell, and using ohmic drop compensation. The working electrode was a steady glassy carbon electrode of 0.8 or 3.1 mm² surface area, the counter electrode was a platinum wire and the reference was a Ag/AgCl (KCl 3 M) electrode separated from the solution by a bridge. The CVs were recorded in extra dry dichloromethane from Sigma-Aldrich, using a Metrohm PGSTAT100N potentiostat controlled by the Nova 2.1.4 software. The electrolyte salt, tetrabutylammonium tetrafluoroborate ($TBABF_4$), was recrystallized and all the glassware was carefully dried before use. Other supporting electrolytes were purchased from commercial suppliers and used without further purification.

Section S8 : Analysis of the voltammetry of $\mathbf{1}^{2+}\cdot 2Cl^-$ at multiple scan rates

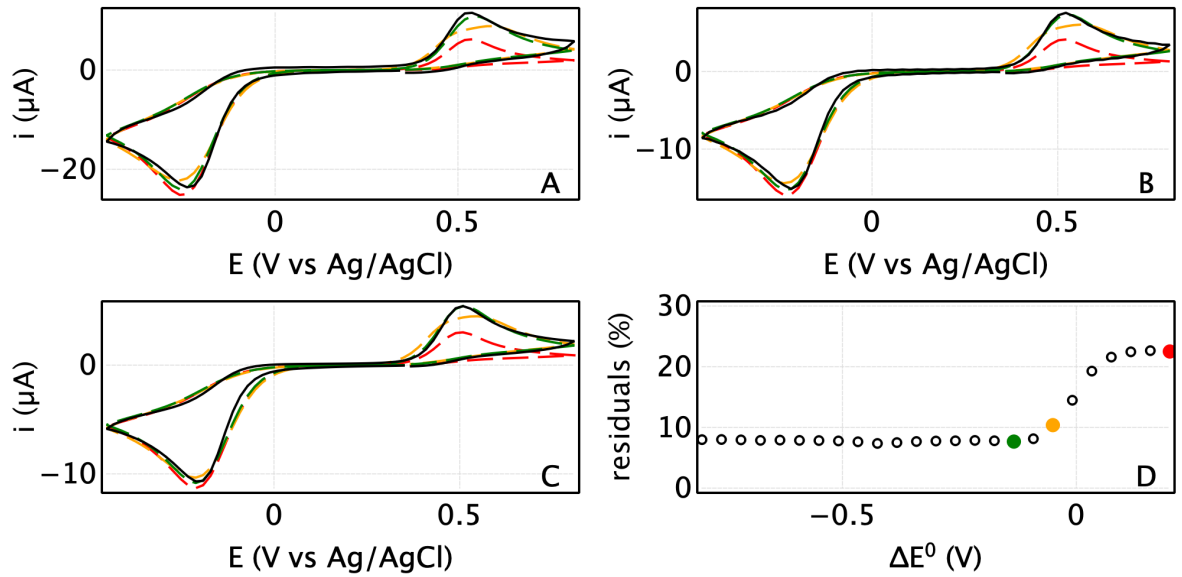

Figure S7. Simultaneous fit of the CVs recorded with $Ni(BQ)_2Cl_2$ ($\mathbf{1}^{2+}\cdot\mathbf{2Cl}^-$) in CH_2Cl_2 + $TBABF_4$ at three different scan rates. Panels A-C each show three particular fits obtained by forcing ΔE^0=-133 mV (green), -50 mV (orange) or 200 mV (red), $\alpha_1 = 0.5$, $\alpha_2 = 0.3$, $D = 9\ 10^{-6}$ cm²/s and adjusting $(E^0_1+E^0_2)/2$, k_{01}, k_{02}, and AC. Each panel shows a CV recorded at a certain scan rate (A: 5V/s, B: 2V/s, C: 1V/s). Panel D shows the total residue as a function of ΔE^0. The quality of the fit is as good as above, the dependence on scan rate is well reproduced, and, again, we conclude that all values of ΔE^0 lower than about -90 mV are consistent with the voltammetry.

Section S9 : Voltammetry of $1^{2+}\cdot 2Cl^-$ in CH_2Cl_2+TBACl

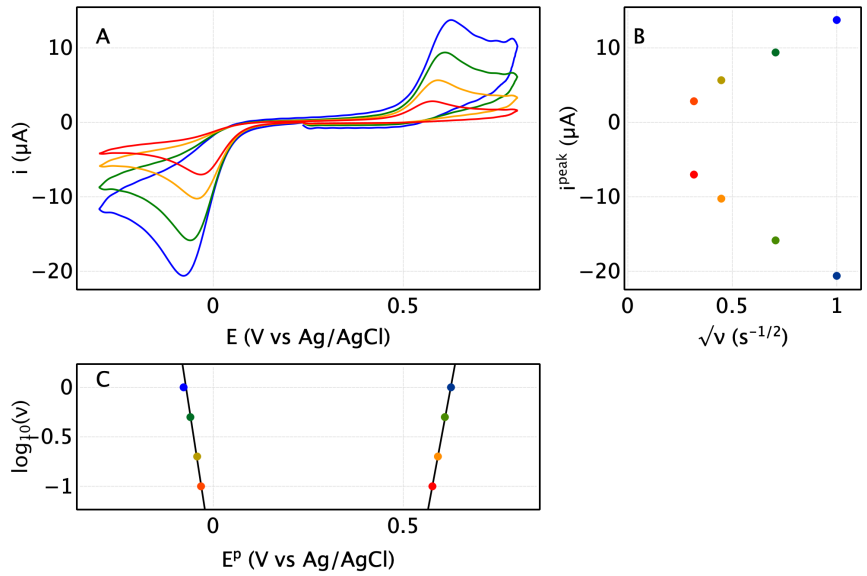

Figure S8. Voltammetry of $NiBQ_2Cl_2$ ($\mathbf{1^{2+}\cdot 2Cl^-}$) in 1 mM in CH_2Cl_2 and 0.1 M TBACl.
Panel A: CVs recorded in the range 0.1 to 1V/s (from red to blue).
Panel B: the linear change in peak current against square root of scan rate.
Panel C: trumpet plot of peak positions against scan rate on a log scale. From the fits of a straight line to each branch of the trumpet plot, we calculated $\alpha_2 = 0.26$ and $\alpha_1 : 0.56$.
T = 25°C, glassy carbon, A = 3.1 mm^2, C = 1 mM.

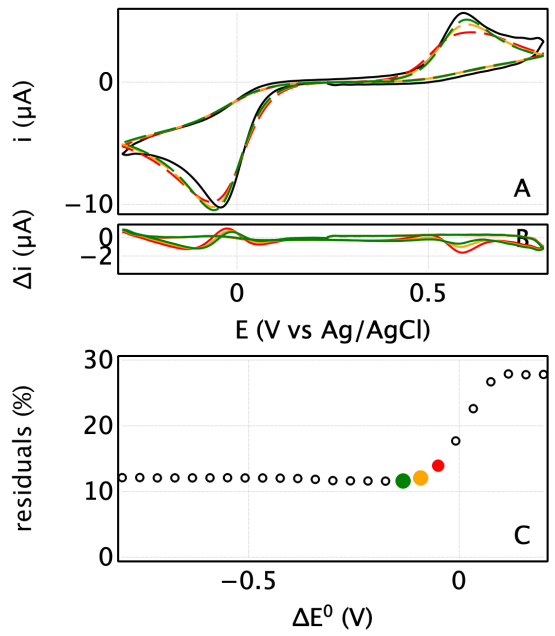

Figure S9. The analysis in fig. 10 is repeated with the 0.2V/s CV shown in Fig S6, obtained with the $NiBQ_2Cl_2$ complex ($\mathbf{1^{2+}\cdot 2Cl^-}$) in CH_2Cl_2+ TBACl.

Section S10 : Voltammetry of 1 in CH_2Cl_2+TBACl

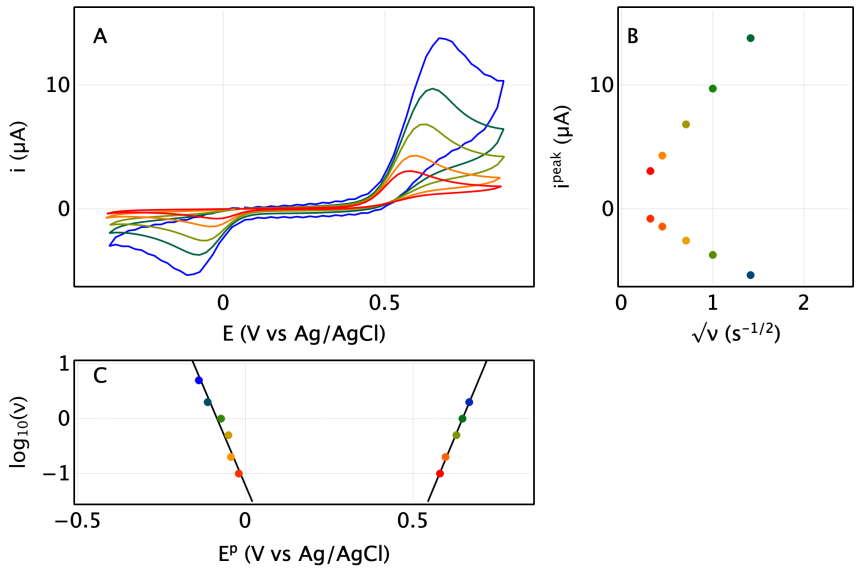

Figure S10. Voltammetry of $Ni(SQ)_2$ (**1**) in 1 mM in CH_2Cl_2 and 0.1 M TBACl. Panel A: CVs recorded in the range 0.1 to 2V/s (from red to blue). Panel B: the linear change in peak current against square root of scan rate. Note that in this voltammetry of the reduced complex, the anodic peak is larger than the cathodic peak, in contrast to e.g. the results in fig S7. Panel C: trumpet plot of peak positions against scan rate on a log scale. From the fits of a straight line to each branch of the trumpet plot, we calculated $\alpha_2 = 0.56$ and $\alpha_1 : 0.43$. T = 25°C.

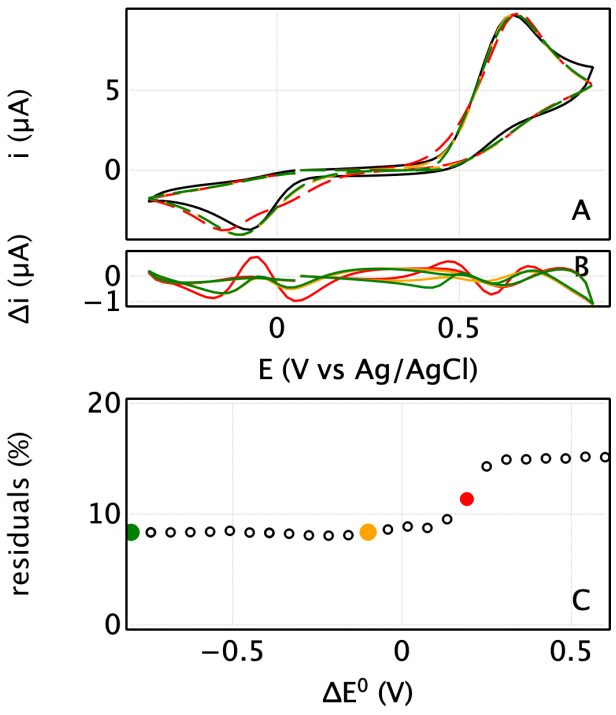

Figure S11. The analysis in fig. 10 is repeated with the 1V/s CV shown in Fig S9, obtained with the $Ni(SQ)_2$ complex (**1**) in CH_2Cl_2+ TBACl.

Section S11: Further discussion of eq 16 and fig 6C

For the various sets of parameters that give the same peak separation ΔE^p, eqs 10 and 11 can be combined to show that the exact relation between ΔE^0 and k_{01}, k_{02}, α_1 and α_2 should be

$$E_1^0 - E_2^0 = -\Delta E^p + \underbrace{\frac{RT}{\alpha_1 F}\left(0.780 + \ln\sqrt{\frac{D_O \alpha_1 F \nu}{k_{01}^2 RT}}\right) + \frac{RT}{(1-\alpha_2)F}\left(0.780 + \ln\sqrt{\frac{D_R (1-\alpha_2) F \nu}{k_{02}^2 RT}}\right)}_{X}$$

Figure S12 shows the best value of ΔE^0 plotted against the value of X calculated form the best values of k_{01}, k_{02}, α_1 and α_2 for the 100 best fits discussed in relation to figure 6D. The series of data points in a line of slope unity, offset by $-\Delta E^p$=-0.75V, as predicted by the equation above.

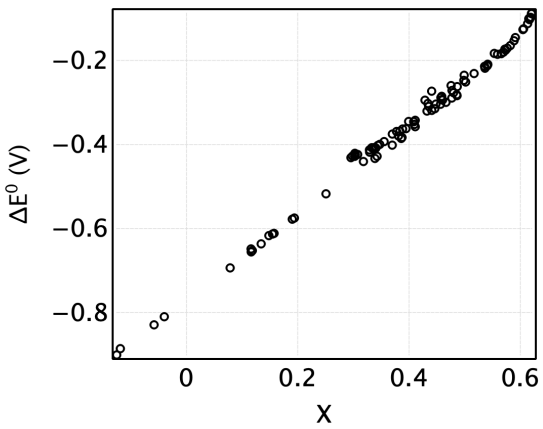

Figure S12. The best value of ΔE^0 plotted against the value of X calculated form the best values of k_{01}, k_{02}, α_1 and α_2 for the 100 best fits discussed in figure 6D.

Section S12: Peak positions for *surface-confined* two-electron species when potential inversion occurs

In the case $E^0_1 < E^0_2$ and in the irreversible limit, and assuming that $\alpha_1 \approx \alpha_2$ and $k_{01} \approx k_{02}$, the peak on the reductive sweep occurs at

$$E^{\mathrm{pc}} = E_1^0 - \frac{RT}{\alpha_1 F} \ln \frac{\alpha_1 F \nu}{k_{01} RT} \quad \text{(eq s1)}$$

This reduction of **O** to **I** is followed by the reduction of **I** to **R**, and we expect this second step to be fast because of the very favorable thermodynamics. Therefore the second reduction (**I** to **R**) does not appear as a distinct peak on the reductive sweep.

On the return, anodic sweep, a unique peak is seen when **R** is reoxidized to **I**, and it is followed by the favorable and irreversible oxidation of **I** to **O**.

$$E^{\mathrm{pa}} = E_2^0 + \frac{RT}{(1-\alpha_2)F} \ln \frac{(1-\alpha_2) F \nu}{k_{02} RT} \quad \text{(eq s2)}$$

The requirement that $E^{pc} < E^{pa}$ gives the order of magnitude of the scan rate above which the peaks split. Assuming again that $\alpha_1 = \alpha_2$ and $k_{01} = k_{02}$, we obtain

$$\nu_{\mathrm{split}} = \frac{k_0 RT}{\alpha F} \exp\left(\frac{\alpha F}{2RT} (E_1^0 - E_2^0) \right) \quad \text{(eq s3)}$$

which is all the smaller the potentials are crossed, and may be much smaller than $k_0 RT/\alpha F$.

The peak separation $\Delta E_p = E_p^{\text{anodic}} - E_p^{\text{cathodic}}$ (obtained from eqs s1 and s2) has a large thermodynamic contribution $E^0_2 - E^0_1$, and a kinetic contribution that depends on scan rate. For example, if we assume for simplicity that $k_{02} = k_{01}$, $\alpha_1 = \alpha_2 = 0.5$, we deduce from eqs s1 and s2:

$$\Delta E_p = \underbrace{E_2^0 - E_1^0}_{\text{thermodynamics}} + \underbrace{\frac{2RT}{\alpha F} \ln \frac{\alpha F \nu}{k_0 RT}}_{\text{kinetics}} \quad \text{(eq s4)}$$

The sign of the kinetic contribution may be positive or negative, and therefore the peak separation can be greater or lower than ΔE^0, it is not a proxy of the potential inversion:

$$\Delta E^p \neq -\Delta E^0 \quad \text{(eq s5)}$$

Regarding the interpretation of the trumpet plots in the case of cooperative ET, the values of k_{01} and k_{02} cannot be deduced from the value of the scan rate above which the peaks split unless ΔE^0 is known. The slopes of the two branches of the trumpet plot (around 120 mV/decade if $\alpha \approx 0.5$) are :

$$\mathrm{d}\ E^{\mathrm{pc}} / \mathrm{d}\ \log_{10}(\nu) = -2.3RT/\alpha_1 F \quad \text{(eq s6)}$$

$$\mathrm{d}\ E^{\mathrm{pa}} / \mathrm{d}\ \log_{10}(\nu) = 2.3RT/(1-\alpha_2)F \quad \text{(eq s7)}$$

Last, in this irreversible limit where peak positions depend on scan rate, the average of the peak positions equates the average two electron potential $E^0_m = (E^0_1 + E^0_2)/2$ only on condition that $\alpha_1 = 1 - \alpha_2$ and $k_{01} = k_{02}$ However, in the general case,

$$(E^{\mathrm{pa}} + E^{\mathrm{pc}})/2 \neq (E_1^0 + E_2^0)/2 \quad \text{(eq s8)}$$